Behaviour of Quiet Time Ionospheric Disturbances at African Equatorial and Midlatitude Regions

A thesis submitted in fulfilment of the academic requirements of the degree of

DOCTOR OF PHILOSOPHY

of

RHODES UNIVERSITY

Department of Physics and Electronics

by

Nicola Diane Orford

December, 2017

Abstract

Extreme ionospheric and geomagnetic disturbances affect technology adversely. Pre-storm enhancements, considered a potential predictor of geomagnetic storms, occur during quiet conditions prior to geomagnetic disturbances. The ionosphere experiences general disturbances during quiet geomagnetic conditions and these Q-disturbances remain unexplored over Africa. This study used TEC data to characterize the morphology of Q-disturbances over Africa, exploring variations with solar cycle, season, time of occurrence and latitude.

Observations from 10 African GPS stations in the equatorial and midlatitude regions show that Q-disturbances in the equatorial region are predominantly driven by $\mathbf{E} \times \mathbf{B}$ variations, while multiple mechanisms affect the midlatitude region. Q-disturbances occur more frequently during nighttime than during daytime and no seasonal trend is observed. Midlatitude Q-disturbance mechanisms are explored in depth, considering substorm activity, the plasmaspheric contribution to GPS TEC and plasma transfer between conjugate points.

Substorm activity is not a dominant mechanism, although Q-disturbances occurring under elevated substorm conditions tend to have longer duration and larger amplitude than general Q-disturbances. Many observed Q-disturbances become non-significant once the plasmaspheric contribution to the TEC measurements is removed, indicating that these disturbances occur within the plasmasphere, and not the ionosphere. Transfer of plasma between conjugate points does not seem to be a mechanism driving Q-disturbances, as the corresponding nighttime behaviour expected between depletions in the summer hemisphere and enhancements in the winter hemisphere is not observed.

Pre-storm enhancements occur infrequently, rendering them a poor predictor of geomagnetic disturbances. Pre-storm enhancement morphology does not differ significantly from general quiet time enhancement morphology, suggesting pre-storms are not a special case of Q-disturbances.

Contents

List of Figures **iv**

List of Tables **vi**

1 Introduction **1**

1.1 Thesis Objectives 4

1.2 Thesis Outline 4

2 Theoretical Background **6**

2.1 The Ionosphere 6

2.1.1 The D-layer 7

2.1.2 The E-layer 8

2.1.3 The F-layer 9

2.1.4 Topside Ionosphere 9

2.2 Ionospheric Morphology 10

2.2.1 Latitudinal Variability 10

2.2.2 Diurnal Variability 11

2.2.3 Seasonal Variability 11

2.2.4 Solar Cycle Variability 13

2.3 Quiet Time Disturbances 13

2.4 Geomagnetic Disturbances 15

2.5 Pre-storm Enhancements 17

2.6 The Plasmasphere 18

2.7 Summary 21

3 Instrumentation and Analysis **23**

3.1 Instrumentation 23

3.1.1 Global Positioning System 23

3.1.1.1 Total Electron Content 24

3.1.2 COSMIC 30

3.1.2.1 PodTec 31

3.1.3 Magnetometer 35

3.1.3.1 Dst Index 37

3.1.3.2 Kp Index 38

3.1.3.3 AE Index 38

3.2 Data Analysis 39

3.2.1 Q-disturbances 39

3.2.2 Plasmaspheric Contribution to TEC 42

3.3 Summary 45

4 Morphology of Q-disturbances over African Latitudes **47**

4.1 Total Number of Q-disturbances 48

4.2 Duration of Q-disturbances 52

4.3 Q-disturbance Amplitude 53

4.4 Discussion 55

4.5 Summary 60

5 Q-disturbances - Midlatitude Mechanisms **61**

5.1 Substorm Activity and Q-disturbances 61

5.2 The Role of the Plasmasphere 67

5.2.1 Ionospheric TEC 68

5.2.2 Plasmaspheric Transfer between Conjugate Points 70

5.3 Summary 74

6 Pre-storm and Quiet Time Enhancements **75**

6.1 Summary 78

7 Summary and Future Work **80**

7.1 Q-disturbance Morphology 80

7.2 Mechanisms in the Midlatitude Region 82

7.3 Pre-storm Enhancements 83

7.4 Future Work 83

8 References **86**

List of Figures

2.1 Atmospheric temperature profile of the upper atmosphere with ionospheric electron density profile. 6
2.2 Typical vertical profile of electron density in the ionosphere at solar minimum and solar maximum during the daytime and nighttime. 8
2.3 Variation of ionospheric TEC during 2009 over HNUS, showing typical seasonal variation of the ionosphere. 12

3.1 Schematic depiction of the geometry used in mapping STEC to VTEC. 30
3.2 Schematic depiction of the mapping function used to convert STEC to VTEC for the plasmasphere. 34
3.3 Schematic depiction of the components of the Earth's magnetic field. 35
3.4 A plot of the temporal variation of the Dst, Kp and AE indices. 37
3.5 Map of GPS stations used in determining the morphology of Q-disturbances over Africa. 40
3.6 Illustration depicting the IPP and PPP. 44

4.1 Ionospheric variation at EMLO during September-October 2009. 48
4.2 Total number of Q-disturbances observed. 49
4.3 Monthly occurrence of Q-disturbances. 51
4.4 Duration of Q-disturbances. 52
4.5 Amplitude of Q-disturbances. 54

5.1 Q-disturbance amplitude under disturbed subauroral conditions. 64
5.2 Q-disturbance duration under disturbed subauroral conditions. . 66
5.3 Number of Q-disturbances at PENC, TUBI, HNUS and SPRT for 2009. 70
5.4 Number of Q-disturbances at conjugate stations per region as a percentage occurrence per season. 71
5.5 Schematic depiction of thermospheric winds. 72
5.6 Seasonal Q-disturbance occurrence at conjugate stations. 73

List of Tables

3.1 Geographic and geomagnetic longitude and latitude of the GPS stations used. 40

5.1 Occurrence of Q-disturbances under disturbed subauroral conditions. 62

5.2 The median total number of Q-disturbances per station and the corresponding percentage of Q-disturbances occurring under disturbed subauroral conditions in each time sector. 63

5.3 Conjugate station coordinates. 68

5.4 Percentage of Q-disturbances which become non-significant after the plasmaspheric TEC has been removed. 68

5.5 Maximum and average percentage contribution of plasmaspheric TEC to Q-disturbances. 69

6.1 Occurrence of pre-storm enhancements. 76

Declaration - Publications

Details of publications that form part and/or include research presented in this thesis.

Signed: _____

1.

Title: Morphology of Quiet Time Disturbances over African Latitudes

Status: In Submission, Journal of Atmospheric, Solar and Terrestrial Physics

Authors: N. Orford, Z. Katamzi-Joseph and D. Burešová

Description: This paper describes the morphology of Q-disturbances over the African region. It outlines the methods used in extracting Q-disturbances, presents the morphology observed over the African region and discusses the implications of the observed morphology on the mechanisms proposed in literature. This paper is discussed in Section 3.2.1 and Chapter 4.

Acknowledgements

I would like to thank my supervisor, Dr Zama Katamzi-Joseph, for her help and guidance. I would like to thank the South African National Space Agency for the financial support and facilities, as well as the individuals within SANSA, without whom this thesis would never have been completed. I would also like to thank Dalia Burešová for the valuable discussions and input she provided.

My eternal gratitude goes to my family, who have in every way made my thesis possible. To my parents, who have taught me that no matter what, we will make a plan. To my fiancé, Ryan for moving across the country with me and for all the sacrifices that went into helping me complete this thesis. Finally, to my sister Tarryn, for proofreading my thesis and giving all the support only a sister can give.

Chapter 1

Introduction

The atmosphere surrounding the Earth comprises many regions, which are categorised by the way that temperature varies within the region, as well as the variation of other properties such as density, composition and degree of ionisation. Two regions of interest for this project are the magnetosphere and the ionosphere. The magnetosphere is the region of the atmosphere whose dynamics are mostly controlled by the Earth's magnetic field (*Davies*, 1989). The ionosphere is a region of the atmosphere comprising a thick shell of electrons and other charged particles or ions. These regions are affected by a phenomenon known as space weather. The term space weather refers to the short term effects (with time scales from minutes to days) that the Sun has on the Earth and other planets.

The ionosphere lies at an altitude of $\sim$ 60-1 000 km. The ionisation of the ionosphere caused by incoming solar radiation affects the transmission of radio waves, making the ionosphere a region of importance (*Davies*, 1989). The magnetosphere lies below L-shell 6-10 on the daytime side of the Earth (*Rishbeth and Garriott*, 1969). Within the magnetosphere, the atmosphere predominantly comprises ions and the movement of these ions is geomagnetically controlled. The magnetosphere is primarily of interest for this study due to the effects it has on the behaviour of the ionosphere. The ionospheric and magnetospheric regions are affected by solar phenomena such as solar flares,

coronal mass ejections, high speed solar winds and solar energetic particles. The Sun and it's associated space weather are the primary drivers of the behaviour of the magnetosphere and ionosphere as well as the interaction of these two regions. Solar storms cause changes in the solar wind, which interacts intensely with the magnetosphere. The ionosphere reacts intensely to the resulting geomagnetic storm or sub-storm resulting in an ionospheric storm. Ionospheric storms are considered an extreme form of space weather and are important as they can have adverse effects on space navigation, high frequency communications and ground based power systems, as discussed in *Fisher and Kunches* (2011) and *Schrijver et al.* (2015) for example.

The response of the ionosphere to geomagnetic disturbances has been widely studied, for example *Buonsanto* (1999); *Danilov* (2001); *Mendillo* (2006). A phenomenon, which sometimes occurs prior to ionospheric storms is an ionospheric enhancement, often referred to as a pre-storm enhancement. This pre-storm 'reaction' of the ionosphere has not been as deeply studied as ionospheric storms themselves (*Burešová and Laštovička*, 2008; *Danilov*, 2013). The phenomenon of pre-storm enhancements was first described by *Kane* (1973). *Kane* (1973) noted extreme changes in the ionosphere observed from several hours before the onset of the geomagnetic storm and these changes of the ionosphere preceding the geomagnetic disturbance form the phenomenon now referred to as a pre-storm enhancement. An understanding of the sources of pre-storm enhancements could indicate whether pre-storm enhancements could be used in forecasting storm effects on the ionosphere (*Burešová and Laštovička*, 2007). However, despite several studies on pre-storm enhancements, e.g. *Adekoya et al.* (2012); *Blagoveshchensky and Kalishin* (2009); *Burešová and Laštovička* (2007, 2008); *Chukwuma* (2010); *Liu et al.* (2008b), the mechanism driving these disturbances is still poorly understood.

In order to be certain that the observed pre-storm enhancement is not due to prior geomagnetic or ionospheric disturbances, the pre-storm enhancement

must be observed under quiet conditions (*Mikhailov and Perrone*, 2009). The ionosphere is however, known to exhibit disturbances under quiet time conditions unrelated to geomagnetic disturbances and ionospheric storms (hereinafter Q-disturbances). *Mikhailov and Perrone* (2009) thus caution that it is important to determine whether pre-storm enhancements are in fact Q-disturbances that coincidentally occur prior to a geomagnetic disturbance event or whether they are a separate type of ionospheric event. In order to do this, the morphology of the more frequently observed Q-disturbances must be understood in order to determine whether the morphology of the less frequent pre-storm enhancements differs in any significant way. This will allow us to determine whether pre-storm enhancements differ from quiet time enhancements in any characteristic way and give insight into whether pre-storm enhancements are a separate phenomenon from Q-disturbances. The comparison of Q-disturbance and pre-storm characteristics will also give insight on whether pre-storm enhancements show potential as a prediction mechanism for ionospheric storms.

It is important to note that the mechanisms driving Q-disturbances are themselves poorly understood (*Farelo et al.*, 2002; *Mikhailov et al.*, 2012). These mechanisms are important to understand as improved knowledge of the quiet time behaviour of the ionosphere can help create improved ionospheric models as well as improve prediction of ionospheric disturbances. Q-disturbances have been studied in a number of regions and under varying conditions, e.g. *Depuev et al.* (2008); *Farelo et al.* (2002); *Liu et al.* (2008a); *Mikhailov et al.* (2004, 2012), but little attention has been paid to this phenomenon over the African region and this study will help to build the global picture of the morphology of Q-disturbances as well as give insight into the mechanisms driving Q-disturbances.

1.1 Thesis Objectives

In this thesis we explore three main topics in order to further the understanding of the behaviour of the ionosphere. These avenues of study are:

- characterise the morphology of Q-disturbances over African latitudes,
- determine whether pre-storm enhancements are Q-disturbances that coincidentally occur prior to geomagnetic disturbances or are a separate phenomenon, and
- explore the mechanisms driving the occurrence of Q-disturbances.

1.2 Thesis Outline

This thesis comprises seven chapters. In Chapter 1 we outlined the background for the problem and identify the questions addressed in the thesis. Chapter 2 forms a literature review in which we will discuss the ionosphere as well as the various mechanisms that drive the characteristic behaviours of the ionosphere. We will also explore the existing research on Q-disturbances and pre-storm enhancements. We introduce geomagnetic disturbances and their role in the behaviour of the ionosphere. Finally, we introduce the plasmasphere.

In Chapter 3 we will discuss the instruments and indices used in our analyses. We will define total electron content (TEC) as our primary measure of the behaviour of the ionosphere, as well as the algorithms used to measure TEC using Global Positioning System (GPS). We will discuss our choice of parameters by which we define quiet time and the methods used in classifying Q-disturbances. We will introduce the Constellation Observing System for Metrology, Ionosphere and Climate (COSMIC) satellite array and the methods used to give us insight into the contribution of the plasmasphere to GPS TEC measurements. Chapter 4 presents the morphology of Q-disturbances over the African region, as well as discussing the insights obtained through

these observations about the mechanisms driving Q-disturbances.

In Chapter 5 we will explore three possible drivers of Q-disturbances in the midlatitude region in greater depth. These mechanisms are substorm activity, plasmaspheric contribution to GPS TEC and plasmaspheric transfer between conjugate points. We will give insight into whether these mechanisms are drivers of the Q-disturbances observed over the African midlatitude region. In Chapter 6 we consider the characteristics of pre-storm disturbances observed during our period of interest and compare these to the observed morphology of Q-disturbances in general. We will discuss the implications of this on whether pre-storm enhancements can be considered a separate phenomenon to Q-disturbances. Chapter 7 will summarise the conclusions of this work, as well as discuss future work.

Chapter 2

Theoretical Background

2.1 The Ionosphere

The ionosphere can be defined as the portion of the atmosphere in which there is sufficient ionisation to affect the propagation of radio waves, as illustrated in Figure 2.1. The ionosphere lies between ~50 km and ~1 000 km and is formed by the interaction of the Sun with the atmosphere (*McNamara*, 1991). Specifically, extreme ultra violet and X-ray radiation from the Sun interact with the neutral atmosphere, forming the ionosphere. This interaction of solar radiation with the neutral atmosphere is known as photoionisation and generates charged particles through the stripping of electrons from neutral atoms,

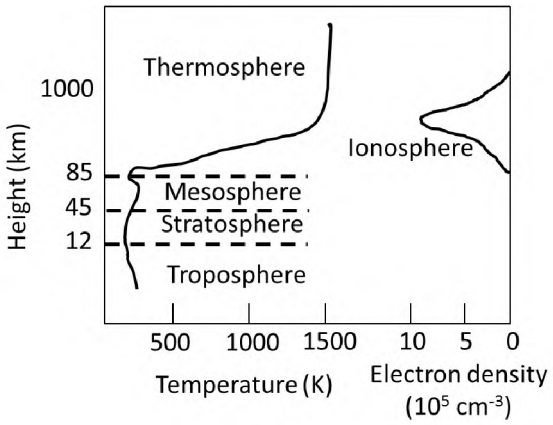

Figure 2.1: Atmospheric temperature profile of the upper atmosphere with ionospheric electron density profile. Figure adapted from *Hargreaves* (1992).

forming charged ions. The ionosphere also undergoes a process called recombination, whereby electrons and ions combine to form neutral atoms.

The effectiveness of the photoionisation process in generating charged particles depends on both the energy of the solar radiation and the density of the surrounding atmosphere (*McNamara*, 1991). In the upper region of the ionosphere, the solar radiation is strong but the atmospheric density is low and therefore the photoionisation process is non-dominant. The intensity of the incoming solar radiation will decrease as altitude decreases due to the absorption of energy through ionisations at higher altitudes. Thus towards the bottom of the ionosphere, although the atmospheric density is high, photoionisation is again non-dominant due to the low energy of the radiation. These variations in density, in predominant molecule depending on height range and intensity of incoming solar radiation with altitude allow the subdivision of the ionosphere into different regions, known as the D-, E- and F-layers and the topside ionosphere, as illustrated in Figure 2.2.

2.1.1 The D-layer

The D-layer occurs at ~50-90 km altitude and forms the lowest layer of the ionosphere (*Rishbeth and Garriott*, 1969). This region comprises a dense neutral atmosphere and is only weakly ionised, as the energy of the incoming radiation is attenuated in the upper layers of the ionosphere. The main sources of ionisation for this region are X-rays, cosmic rays and solar Lyman α (*McNamara*, 1991). Solar Lyman α radiation ionises only NO. Other important species in the region are N_2 and O_2, which are ionised by X-rays and extreme ultra violet. Cosmic rays are especially important during solar minimum, while X-rays produced during a sufficiently strong solar flare penetrate to the D-layer, resulting in a significant increase in ionisation.

The D-layer is a significant source of attenuation for high frequency radio

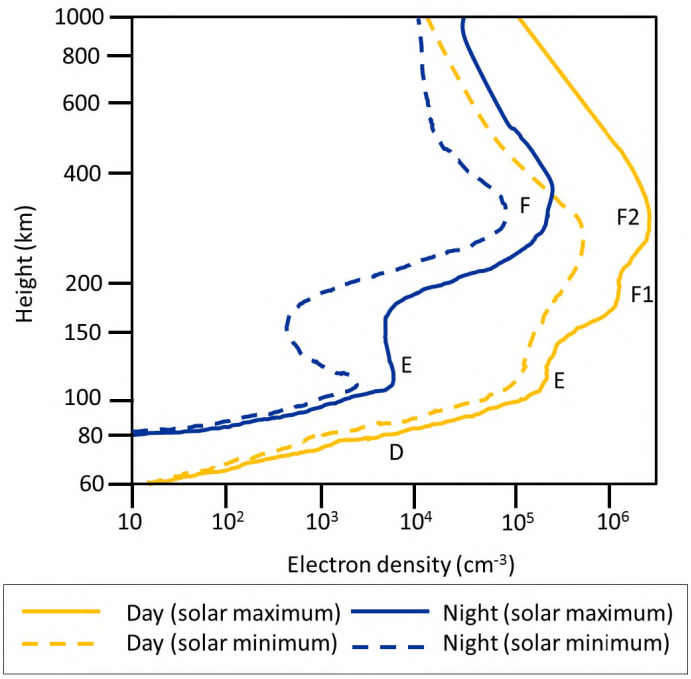

Figure 2.2: Typical vertical profile of electron density in the ionosphere at solar minimum and solar maximum during the daytime and nighttime. Figure adapted from *Hargreaves* (1992).

waves due to the high rates of collision between electrons and the dense neutral atmosphere (*McNamara*, 1991). The increase in ionisation during a solar flare can thus result in complete absorption of radio waves, known as short-wave fadeout. The weak ionisation of the D-region provides only a negligible contribution to the TEC of the ionosphere. The D-region experiences high recombination rates due to the highly collisional, weakly ionised composition. The high recombination rate means the D-layer is mostly present during the day and generally disappears at night.

2.1.2 The E-layer

The E-layer lies at ~90-120 km (*Rishbeth and Garriott*, 1969). The dominant ionisation sources in this layer are low energy X-rays and ultraviolet radiation that have passed through the upper layers of the atmosphere. The dominant molecules N_2, O_2 and O ionise to form N_2^+, O_2^+ and O^+. The E-layer also expe-

riences short lived ionisation sources such as auroral and dynamo electric fields, which cause high electron density areas within the E-layer. These regions of increased density are localised and have a short lifetime. This phenomenon is known as sporadic E and can cause the reflection of high frequency radio waves. The ionisation strength of the E-layer is lower during the nighttime.

2.1.3 The F-layer

The F-region lies above ~120 km and is formed primarily through the ionisation of atomic oxygen by extreme ultra violet radiation (*Rishbeth and Garriott*, 1969). During the daytime, this layer splits into two distinct layers, namely the F1- and F2-layers, which collapse to a single layer during the night due to recombination. During the daytime, the F2-layer has the highest electron density in the ionosphere, whilst at night the F-layer has the highest electron density. The F1-layer has it's peak electron density around ~200 km altitude, while the F2-layer has it's peak around ~300 km (*McNamara*, 1991). This layer is the most important layer for high frequency radio communications, allowing communication over the horizon (*Davies*, 1989). The F-layer is also the largest contributor to ionospheric TEC, since it has the highest levels of ionisation. This layer can be strongly affected by geomagnetic disturbances, but responds differently to the lower ionosphere (*Danilov*, 2013).

2.1.4 Topside Ionosphere

The topside ionosphere lies above the F2-layer peak and extends to ~1 000 km (*Rishbeth and Garriott*, 1969). This region experiences less photoionisation than the F-layer due to it's low atmospheric density and has a sharp decrease in electron density with altitude. The dominant ions in this region are H^+ and O^+.

2.2 Ionospheric Morphology

The characteristics of the ionosphere vary diurnally as well as with latitude, season and solar cycle. This variability will be explored below.

2.2.1 Latitudinal Variability

The dominant mechanisms driving behaviour in the ionosphere are strongly linked to geomagnetic latitude. The ionosphere can be split into low, mid and high latitude regions, with the low and midlatitude regions forming the areas of interest in this thesis.

The low latitude or equatorial regions lie below 20° geomagnetic latitude. Ionospheric behaviour in this region is dominantly determined by a vertical electromagnetic drift resulting from the interaction of charged electrons and the Earth's magnetic field (*Davies*, 1989). This drift is known as vertical $\mathbf{E}\times\mathbf{B}$ plasma drift. The vertical $\mathbf{E}\times\mathbf{B}$ drift is responsible for the fountain effect, which causes electrons to experience upwards drift at the equator and to move towards higher altitudes, where they descend along the magnetic field lines, due to the force of gravity, and settle at ∼15° North and South of the geomagnetic equator. This results in a region of low electron density at the magnetic equator and regions of high electron density at ∼15° North and South of the geomagnetic equator (*Davies*, 1989). These regions are often referred to as the equatorial trough and crests, respectively, and are referred to as the equatorial ionisation anomaly. As ionisation levels are affected by the direction of incoming radiation, regions that have a low solar zenith angle will have higher levels of photoionisation. This means that the low latitude regions have higher electron densities than other latitude regions.

The midlatitude region lies between 20°-60° North and South of the geomagnetic equator. This region is dominantly controlled by the balance between photoionisation and recombination. Thermospheric winds also play a signif-

icant role in the midlatitude region. The electron density gradient is not as steep in this region as in the low and high latitude regions (*McNamara*, 1991).

The behaviour of the ionosphere in the high latitude regions, above 60°, is very complex, as it is linked to both the magnetosphere and the interplanetary medium. As the African sector will be primarily studied, the high latitude regions are not studied directly in this thesis. Further details of the behaviour of this region can be found in *Davies* (1989), *McNamara* (1991) and *Rishbeth and Garriott* (1969).

2.2.2 Diurnal Variability

The solar zenith angle determines the path length of ionising radiation through the atmosphere. At low solar zenith angles, the radiation intensity per unit area is higher, thus towards midday, the radiation is more direct in the low and midlatitude regions and a higher rate of photoionisation results. At high solar zenith angles, energy is dissipated along the ray path through the atmosphere and less photoionisation occurs. This results in an increasing rate of photoionisation throughout the day until zenith is reached after which the rate of photoionization decreases, until the Sun sets and recombination becomes the dominant process within the ionosphere. This causes a strong diurnal variation of the number of ionised particles within the various layers of the ionosphere, where maximum ionisation is observed during the day, while at night the ionisation is low, as illustrated in Figure 2.2. In addition, the D and F1 layers disappear at night, also illustrated in Figure 2.2.

2.2.3 Seasonal Variability

The solar zenith angle changes seasonally, with lower angles seen during the summer months. This leads to higher levels of ionisation during the summer

months, as shown in Figure 2.3. This seasonal variation is most prominent in the low and high latitude regions. The midlatitude region sometimes experiences what is known as the seasonal anomaly, whereby higher F2-layer electron densities are seen during winter than during summer. The ionospheric electron density is strongly dependent on both the solar zenith angle and the thermospheric composition, especially the atomic/molecular ratio $[O]/[N_2]$. The prevailing summer to winter general circulation leads to higher levels of $[O]/[N_2]$ during winter than during summer, thus higher levels of ionisation occur during winter. Details of the seasonal anomaly can be found in *Davies* (1989), *McNamara* (1991) and *Liu et al.* (2009).

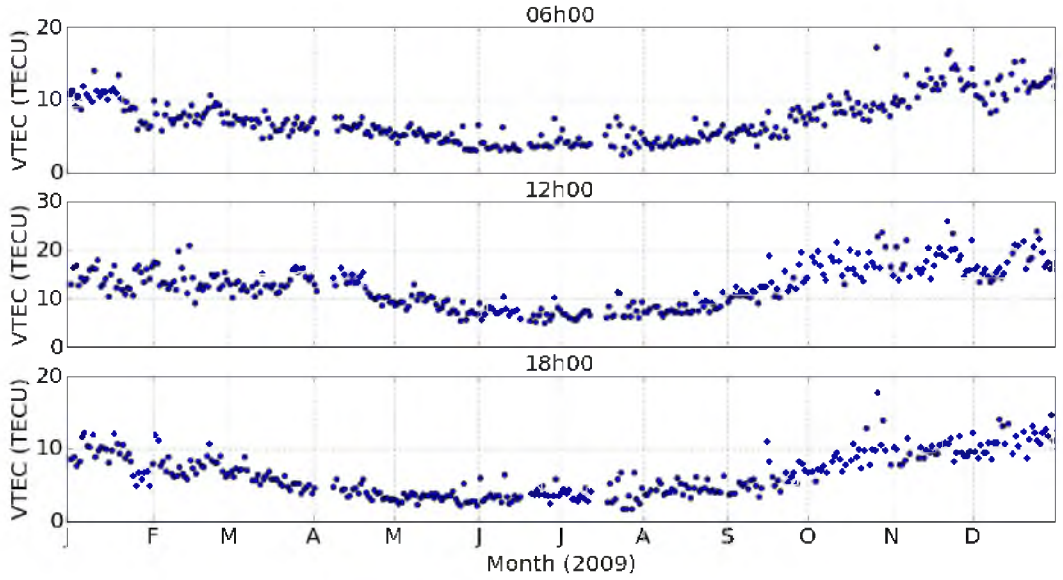

Figure 2.3: Variation of ionospheric TEC in TEC units (TECU) during 2009 over HNUS at 06h00, 12h00 and 18h00, showing typical seasonal variation of the ionosphere.

In addition, the midlatitude region also experiences unexpectedly higher electron densities at the equinoxes than during other seasons, forming a semi-annual anomaly (*Hargreaves*, 1992). This occurs due to symmetry of the thermospheric circulation at the equinoxes, which optimises the effects of thermospheric composition and the solar zenith angle (*Liu et al.*, 2009). The Earth's atmosphere lags two hours behind the rotation of the Earth's surface

in summer, so although the maximum photoionisation occurs around midday, the highest levels of electron density are observed at approximately two hours after local midday, while in winter the highest ionisation levels are observed before local midday (*McNamara*, 1991).

2.2.4 Solar Cycle Variability

The activity of the Sun varies with a cycle of ~11 years duration (*McNamara*, 1991). Variations in the Sun's magnetic field cause dark spots on the surface of the Sun, known as sunspots, where the temperature is lower than the surrounding region. During a solar cycle, large numbers of sunspots are seen during the solar maximum period and sunspots are observed less frequently during the solar minimum period. At solar maximum, there is an increased amount of radiation, which leads to increased photoionisation in the ionosphere and higher electron densities are thus observed, as illustrated in Figure 2.2. The higher activity level of the Sun during solar maximum also results in more frequent geomagnetic disturbances due to solar disturbances such as coronal mass ejections and solar flares, leading to a high number of ionospheric storms during and after solar maximum (*Davies*, 1989).

2.3 Quiet Time Disturbances

Disturbances of the ionosphere unrelated to disturbed geomagnetic activity are known as Q-disturbances. Q-disturbances exist as both positive and negative deviations of the vertical TEC (VTEC) from either a monthly or a 27-day running median. Q-disturbances occur in any time sector under quiet geomagnetic conditions and have been observed extensively. For example, *Depueva et al.* (2005) studied Q-disturbances in the equatorial regions using observations from two ionosonde stations (Huancayo and Kodaikanal) at equatorial latitudes over 3-4 solar cycles, while *Depuev et al.* (2008) used model simula-

tions to interpret the morphological picture revealed in *Depueva et al.* (2005). The morphological picture over the equatorial region presented in *Depueva et al.* (2005) and analysed in *Depuev et al.* (2008), shows both positive and negative Q-disturbances with a systematic dependence on solar activity, season and local time.

Farelo et al. (2002) noted that nighttime enhancements in the midlatitude region show distinct variations between pre- and post-midnight events, suggesting different physical mechanisms driving the formation of these disturbances. Q-disturbances have been found to behave differently in different geomagnetic latitude regions. For example, *Mikhailov et al.* (2004) found that the amplitudes of quiet time enhancements increase with latitude and that quiet time depletions have a latitudinally invariant amplitude.

Although the mechanism(s) driving Q-disturbances are thought to differ from those of F2-layer storm effects related to geomagnetic activity, the mechanisms remain an open question (*Mikhailov et al.*, 2004, 2007). *Depueva et al.* (2005) and *Depuev et al.* (2008) explored the observed morphology of the equatorial region in terms of $\mathbf{E}\times\mathbf{B}$ variations and consider this to be the main driving mechanism of Q-disturbances in this region, because many features of their observations were explained by these variations. However, *Liu et al.* (2008a) explored three events (on 10 February 2004, 21 January 2004 and 4 March 2001) over the Asian/Australian low latitude region in more detail and concluded that they may be related to auroral or magnetospheric activities. The situation in the midlatitude region is more complex and *Farelo et al.* (2002); *Liu et al.* (2008a); *Mikhailov et al.* (2004, 2007, 2009) discuss a number of mechanisms that play a role in forming the overall morphology of Q-disturbances in this latitude region. These mechanisms include neutral composition, plasmaspheric fluxes, thermospheric winds, solar EUV radiation variations and plasmaspheric transfer from conjugate points. Medium scale traveling ionospheric disturbances (MSTIDs) (see for example *Hernández-Pajares et al.* (2012b))

propagate in the ionosphere with periods of several minutes to less than one hour and with velocities of 50-300ms^{-1} and are thus seldom present at a single station to cause an observed disturbance which meets the minimum duration used in this work. Similarly, ionospheric disturbances caused by solar flares (see for example *Hernández-Pajares et al.* (2012a)) have durations of tens of seconds, lying below the minimum duration used in this work. MSTIDs and solar flares will thus not be explored further.

Q-disturbances have been explored over the American, Indian and Eurasian sectors and a complex morphology has been revealed, suggesting geophysical conditions have a large influence on the mechanisms of formation. The African sector however, remains under-explored. Analysis of the morphology of Q-disturbances over Africa allows further understanding of the influence of vertical plasma drift through comparison of the morphology of the equatorial region to the results of *Depuev et al.* (2008); *Depueva et al.* (2005). Analysis of the morphology over the midlatitude sector allows comparison to the different formation mechanisms suggested in *Farelo et al.* (2002); *Mikhailov et al.* (2004, 2007).

2.4 Geomagnetic Disturbances

The ionosphere is affected by changes in the Earth's geomagnetic field. A brief introduction to geomagnetic storms and substorm behaviour is thus given. The creation of an enhanced ring current can be considered the key defining property of a geomagnetic storm. This ring current is precipitated by the influx of highly energetic solar particles transported by the solar wind. These highly energetic particles interact with the Earth's magnetic field, filtering down to the ionosphere. This interaction results in an enhancement of the ring current, with ions and electrons in the range of 10-300 KeV located between 2-7 Earth radii (*Gonzalez et al.*, 1994). This enhanced ring current produces a

geomagnetic disturbance or geomagnetic storm. A geomagnetic storm forms a significant departure from standard behaviour of the magnetosphere and ionosphere, resulting in enhanced electric and magnetic fields. The duration of geomagnetic storms can be from one to several days. Geomagnetic storms can result in phenomena such as energetic particle precipitation and intense variations of electron density and content.

Geomagnetic storms comprise three phases, namely the initial, main and recovery phases. During the initial phase, arrival of the solar wind causes compression of the magnetosphere. This results in an increase in magnetic field strength, with a duration of several hours. The main phase of the geomagnetic storm comprises a sustained southwards interplanetary magnetic field with a duration of several hours. The recovery phase is usually the longest phase, lasting up to several days, during which there is a slow return to normal conditions.

A substorm occurs when energy from the interaction between the solar wind and magnetosphere is rapidly dumped into the magnetosphere and the ionosphere in the auroral zone (*Gonzalez et al.*, 1994). The duration of a substorm is minutes to hours, with a single event or series of events possible. Substorms are initiated on the nighttime side of the Earth. The energy dumped into the magnetosphere and ionosphere is initially stored in the magnetotail with a small portion dissipated into the ring current and the ionosphere. This causes an enhancement of the ring current as well as auroral particle precipitation and Joule heating. This is followed by the deposition of energetic particles into the ionosphere, known as the expansion phase, whereafter there is a return towards normal conditions during the recovery phase.

2.5 Pre-storm Enhancements

The ionosphere can be strongly disturbed by changes in the geomagnetic field. These ionospheric responses are known as ionospheric storms and represent an extreme form of space weather. This response of the lower ionosphere results in an increase in the electron density of the ionosphere from the quiet time density, except in the F2-layer where the response can be either an increase or a decrease in electron density (*Danilov*, 2013). These are known as positive and negative ionospheric disturbances respectively. *Kane* (1973) noted a positive disturbance of the ionosphere prior to the commencement of the geomagnetic storm. These disturbances are now referred to as pre-storm enhancements and it has been suggested by e.g. *Danilov* (2001) and *Kane* (2005), that the occurrence of pre-storm enhancements could be used to predict geomagnetic disturbances. Pre-storm enhancements have been studied by *Adekoya et al.* (2012); *Blagoveshchensky et al.* (2006); *Burešová and Laštovička* (2008); *Chukwuma* (2010) and *Liu et al.* (2008a) amongst others, but their mechanisms and characteristics are still poorly understood.

Burešová and Laštovička (2007) studied 65 strong geomagnetic storms with a duration of more than 4 hours, between 1995-2005, and found that about 20-25% of these disturbances were accompanied by pre-storm enhancements over the European sector. Furthermore, *Burešová and Laštovička* (2007) found pre-storm enhancements occurring in both daytime and nighttime and noted that pre-storm enhancements had a tendency to be more frequently observed during the summer months, but did not detect any latitudinal dependence on frequency of occurrence. *Burešová and Laštovička* (2008) further noted that pre-storm enhancements are confined to the F2-layer with no corresponding disturbance detected in the E or F1 layers and that pre-storm enhancements are not a global nor a regional phenomenon but have a longitudinal extent of $\sim$120°-240°. *Liu et al.* (2008b) studied pre-storm enhancements over the Asia/Australia sector and found that the observed pre-storm disturbances had

a latitudinal variation, with depletions observed in the equatorial region and maximal enhancements observed near the crests of the equatorial ionization anomaly in the northern and southern hemispheres. This differs from the lack of latitudinal variation in the European sector noted by *Burešová and Laštovička* (2007).

Many mechanisms have been suggested as drivers of pre-storm disturbances. For example, *Danilov and Belik* (1991) suggested that pre-storm enhancements may be initiated by soft particle precipitation in the dayside cusp region, while *Mansilla* (2007) suggested soft particle precipitation at high latitudes. *Kane* (2005) suggested the origin of pre-storm enhancements could be due to coupling from below between the ionosphere and neutral atmosphere, while *Burešová and Laštovička* (2007) suggest that there is no dominant mechanism and that the mechanisms driving individual events may differ. In contrast *Mikhailov and Perrone* (2009) undertook a critical analysis of the observed pre-storm enhancements and stated that "there are no convincing arguments" that the observed ionospheric enhancements at mid and sub-auroral latitudes are related to the subsequent magnetic storm. *Mikhailov and Perrone* (2009) further stated that pre-storm enhancements can be attributed to moderate auroral activity, prior geomagnetic storm activity or positive Q-disturbances (quiet time enhancements) of the ionosphere. It is therefore important to establish whether there can be a clear differentiation between the characteristics of pre-storm enhancements and quiet time enhancements of the ionosphere.

2.6 The Plasmasphere

A number of mechanisms proposed as drivers of Q-disturbances relate to the plasmasphere. These include transfer of electrons along magnetic field lines between hemispheres, disturbances of the plasmasphere, underestimation of the contribution of the plasmasphere to the measured TEC and transfer of ionisa-

tion between the topside ionosphere and the plasmasphere. These mechanisms will be explored more deeply in Sections 3.2.2 and 5.2. The plasmasphere is thus introduced to form a foundation for these later analyses.

The solar wind and the Earth's magnetic field interact, forming the magnetosphere. The magnetosphere is compressed by the solar wind on the day side of the Earth and streams outwards to form an elongated 'tail' on the night side (*Davies*, 1989). Within the magnetosphere, the motion of charged particles is predominantly controlled by the forces exerted by the Earth's magnetic and electric fields. The lower part of the magnetosphere contains cold plasma and rotates with the Earth. This co-rotating region of the magnetosphere forms a large toroidal shape situated above the ionosphere and is known as the plasmasphere.

The plasmasphere begins at an altitude of about 1 000 km and ends at the plasmapause. The plasmapause is highly dynamic and represents the boundary between the plasma controlled by magnetospheric electric fields and the plasma controlled by the electric field co-rotating with the Earth (*Pedatella and Larson*, 2010). In the plasmaspheric region, the density of the neutral atmosphere is so small that it has little effect on the motion of the charged particles. This region comprises lightly ionized particles, primarily hydrogen ions, confined by the Earth's magnetic field. The dominant particles are protons and thus the plasmasphere is often referred to as the protonosphere (*Davies*, 1989). The ion density within the plasmasphere is very low, with density at 1 000 km altitude in the midlatitude region expected to be of the order of 10^{10} m^{-3}, decaying outwards to the plasmapause where a sudden drop of 1-2 orders of magnitude is observed. The plasma in this region has a temperature of around 1 000 K and is considered to be cold.

A minimal amount of ionisation is produced within the plasmasphere itself. Ionisation is typically produced in the ionosphere and undergoes transfer

between the topside ionosphere and the plasmasphere. Diffusion of the solar produced oxygen plasma up the magnetic field occurs during daytime hours. There is an exchange of charge between this oxygen plasma and neutral hydrogen, according to Equation 2.1, resulting in a hydrogen dominated plasma above a transition region.

$$O^+ + H \rightleftharpoons H^+ + O \tag{2.1}$$

The hydrogen ions and electrons forming this hydrogen plasma move upwards along the magnetic field lines to populate the closed plasma flux tubes (*Davies*, 1989). This hydrogen plasma remains in the plasmasphere until after ionospheric sunset, when it diffuses down from the plasmasphere to the lower altitudes of the ionosphere (*Lunt et al.*, 1999a). As the hydrogen plasma reaches lower altitudes, it undergoes charge exchange with neutral oxygen to form oxygen plasma. This oxygen plasma helps maintain the nighttime F region.

The midlatitude regions in the northern and southern hemispheres can be treated as having a common plasmasphere (*Lunt et al.*, 1999a). This is because the plasmasphere is linked by the field lines joining the conjugate hemispheres. The ionosphere thus acts as the source of plasma to the plasmasphere and the plasmasphere forms a mutual reservoir between the two hemispheres, linking the ionosphere between the northern and southern hemispheres. A diurnal exchange of plasma between the plasmasphere and ionosphere occurs (*Bailey et al.*, 1978). This results in transfer of plasma produced in the summer ionosphere along the field lines to the conjugate winter ionosphere.

The length and volume of the plasma tubes are affected by latitude, with very short, low volume plasma tubes close to the geomagnetic equator. The plasmaspheric tube length increases with latitude, and the corresponding increase in volume of the plasma tube with length influences the behaviour of the electron density in the plasmasphere and the underlying ionosphere (*Car-*

penter and Park, 1973). The small volume of plasma tubes with bases at low magnetic latitudes means that they are in rough equilibrium with the ionosphere and have little effect on the behaviour of the ionosphere. At higher latitudes, the volume of the plasmaspheric tubes increase and dayside filling must occur for a longer period before equilibrium exists between the flux tube and the underlying ionosphere. Towards the polar regions, the volume of the plasma tubes becomes so large that equilibrium cannot be reached (*Carpenter and Park*, 1973).

The limit of the plasma tubes that co-rotate with the Earth is known as the plasmapause and this limit varies with local time. Opposition of the co-rotation flow near the Earth and the sunward convection of the magnetosphere driven by the solar wind, result in a bulge of the plasmasphere in the dusk local time sector (*Chappell*, 1972). This sunward convection of the magnetosphere is enhanced during geomagnetic storms, resulting in a contraction of the plasmapause and rapid depletion of the plasmaspheric flux tubes around dusk on the first day of the geomagnetic storm. The flux tubes are then slowly replenished from the underlying ionosphere over a period of many days after the storm (*Carpenter and Park*, 1973). Flux tubes with their bases at high latitudes have large volumes and the time taken to replenish the plasmaspheric plasma in these tubes is greater than the average recurrence time between geomagnetic storms, resulting in a state of partial replenishment.

2.7 Summary

In this chapter, the structure and morphology of the ionosphere was discussed and an introduction to Q-disturbances was given. Geomagnetic storms and substorms were introduced. The role of pre-storm enhancements as a predictor of geomagnetic storms was discussed, together with the literature on this phenomenon. The plasmasphere and it's interaction with the ionosphere was

presented to allow discussion of the role of the plasmasphere in Q-disturbance formation.

Chapter 3

Instrumentation and Analysis

3.1 Instrumentation

3.1.1 Global Positioning System

GPS is a satellite based radio navigation system, operated and maintained by the United States' Department of Defence. GPS comprises three segments, namely the space, control and user segments. The space segment presently comprises 31 satellites, of which at least 24 are operational 95% of the time, orbiting in six orbital planes. These orbits are inclined at 55° to the equator and are separated by 60° in the equatorial plane (*Hofmann-Wellenhof et al.*, 1997). The satellites orbit at an altitude of ~20 200 km, with a period of 11 hours 58 minutes. This configuration is such that a user almost anywhere in the world has at least four GPS satellites in direct line of sight at all times. The control segment comprises a global network of ground facilities, which track, analyse and monitor satellite transmissions and GPS measurements as well as send commands and data to the GPS array, like GPS satellite clock models and orbital parameters. The user segment comprises the antennae and receivers that measure and decode the satellite transmissions to provide information on position and velocity as well as precise timing abilities to the user .

Each GPS satellite continuously broadcasts radio signals. The two frequen-

cies that will be of interest in this work are within the L-band and are referred to as L1 and L2, respectively, with f_{L1} = 1 575.42 MHz and f_{L2} = 1 227.60 MHz (*Hofmann-Wellenhof et al.*, 1997). The coarse/acquisition (C/A) code is modulated on the L1 carrier phase. Each satellite has different C/A codes, with each code nearly orthogonal to all other C/A codes. The precise (P) code modulates both L1 and L2.

The radio signals broadcast by the GPS satellites pass through the ionosphere as they travel to a GPS receiver. To generate the GPS measurements by transforming the apparent time delay of the signals in pseudorange, the propagation velocity of the electromagnetic (EM) signal is assumed to be equal to that of an EM signal in a vacuum. However, the velocity changes, in particular through the interaction of the EM signal with free electrons. Most of this change can be described by the first order approximation of the refractive index, inversely proportional to the squared frequency and proportional to the electron density, which is moreover, variable with time and with a sign dependence, negative (advance) for the phase and positive (delay) for the group (*Hofmann-Wellenhof et al.*, 1997). Moreover as the ionosphere is not uniform, the signals travel through different refractive indices along the ray path. This results in deviations from the straight line path from the satellite to the receiver and the signals arriving at a GPS receiver are delayed relative to the time a straight-line path would have taken. This time delay of the signal can be used to study the composition of the ionosphere.

3.1.1.1 Total Electron Content

TEC is defined as the total number of electrons in a column of unit cross section between the transmitter and receiver and is measured in TECU, where 1 TECU = 10^{16} electrons m^{-2}. TEC is calculated as the line integral of the electron concentration, N_e, along the signal path from satellite to receiver,

represented by:

$$TEC = \int_r^s N_e(R, \theta, \phi, t) dl, \tag{3.1}$$

where R is the radial distance from the Earth's centre, t is the time and θ and ϕ are the longitude and latitude respectively. TEC can be derived from the delay of GPS radio signals. The theory on radio propagation through the ionosphere is necessary in order to understand the relationship between signal delay and TEC.

The refractive index, μ, of the ionosphere is frequency dependent. The complex refractive index, n, can be written in terms of the refractive index and the wave attenuation due to absorption, χ, as:

$$n^2 = (\mu - i\chi)^2. \tag{3.2}$$

The refractive index depends on the angular electron plasma frequency, ω_{pe}, the angular frequency of the propagating radio wave, ω and the angular gyro frequency of the electrons, ω_{ce}. The refractive index also relies on the transverse and longitudinal components of the imposed magnetic fields, Y_T and Y_l, with respect to the direction of wave propagation and the angle between the Earth's magnetic field and the wave propagation path, θ. The angular frequencies depend on the electron plasma frequency, f_{pe}, the electron gyro frequency, f_{ce}, and the radio wave frequency, f, respectively. The refractive index can be given by the Appleton-Hartree formula:

$$n^2 = 1 - \frac{X}{1 - iZ - \frac{Y_T^2}{2(1-X-iZ)} \pm \left[\frac{Y_T^4}{4(1-X-iZ)^2} + Y_L^2\right]^{1/2}}, \tag{3.3}$$

where:

$$\begin{aligned} X &= (\frac{\omega_{pe}}{\omega})^2 \\ Y &= \frac{\omega_{ce}}{\omega} \\ Y_L &= Y\cos\theta \\ Y_T &= Y\sin\theta \\ \omega_{pe}^2 &= (2\pi f_{pe})^2 \\ \omega_{ce}^2 &= (2\pi f_{ce})^2 \\ &= \frac{B_e}{m_e} \\ Z &= \frac{\nu}{\omega}. \end{aligned}$$

In the E- and F-layers of the ionosphere, there is a low density of neutral atoms and collisions between electrons and neutral atoms are negligible (*Davies*, 1989). This means that for high frequency radio waves, the collision term, given by Z and the wave attenuation due to absorption, χ, can be neglected and Equation 3.3 simplifies to:

$$\mu^2 = 1 - \frac{2X\left(1-X\right)}{2(1-X) - Y_T^2 \pm \left[Y_T^4 + 4\left(1-X\right)^2 Y_L^2\right]^{1/2}}. \tag{3.4}$$

Assuming that the magnetic field is negligible leads to:

$$\mu^2 = 1 - X. \tag{3.5}$$

Equation 3.5 can be expanded using the binomial expansion. At GPS frequencies, the higher order terms can be ignored and Equation 3.5 can be approximated as per *Parkinson and Spilker* (1996):

$$\mu \approx 1 - \frac{1}{2}X. \tag{3.6}$$

Then since

$$\begin{aligned} X &= (\frac{\omega_{pe}}{\omega})^2 \\ &= \left(\frac{f_{pe}}{f}\right)^2, \end{aligned} \tag{3.7}$$

and

$$f_{pe} = \frac{N_e e^2}{4\pi^2 m_e \epsilon_0}, \tag{3.8}$$

where e is the charge of an electron, m_e is the mass of an electron and ϵ_0 is the vacuum permittivity. Substituting Equations 3.7 and 3.8 into Equation 3.6 gives:

$$\mu = 1 - 40.31\frac{N_e}{f^2}. \tag{3.9}$$

The relationship between the phase and group refractive indices is given by (*Hofmann-Wellenhof et al.*, 1997):

$$\mu_g = \mu_p + f\frac{d\mu_p}{df}. \tag{3.10}$$

Since μ_p is given by Equation 3.9, the group refractive index can be written as:

$$\mu_g = 1 + 40.31\frac{N_e}{f^2}. \tag{3.11}$$

Equations 3.9 - 3.11 show that $\mu_g > \mu_p$ and thus $v_g < v_p$, since $v = c/\mu$, where c is the speed of light, and v_p and v_g are the phase and group velocities, respectively. This in turn implies that GPS code measurements are delayed and that the measured pseudo ranges are longer than the actual satellite-receiver geometric range. This also implies that the carrier phases are advanced and that the measured carrier phase pseudo ranges are shorter than the actual satellite-receiver geometric range (*Hofmann-Wellenhof et al.*, 1997).

By definition, the measured GPS pseudorange, ρ, along the line of sight

from the satellite, s, to the receiver, r, is given by:

$$\rho = \int_r^s \mu dl, \tag{3.12}$$

while the geometric range, R, is determined by assuming no dispersion, $\mu = 1$:

$$R = \int_r^s dl. \tag{3.13}$$

The difference in path length between the geometric and pseudo ranges is therefore given by the difference of Equations 3.12 and 3.13. Substituting in Equations 3.9 and 3.11 into the path length yields the group delay (Equation 3.14) and phase advance (Equation 3.15):

$$\Delta\rho_g = \frac{40.31}{f^2}\int_r^s N_e dl \tag{3.14}$$

$$\Delta\rho_p = -\frac{40.31}{f^2}\int_r^s N_e dl. \tag{3.15}$$

Substituting Equation 3.1 into Equations 3.14 and 3.15 then gives:

$$\Delta\rho_g = \frac{40.31}{f^2}TEC \tag{3.16}$$

$$\Delta\rho_p = -\frac{40.31}{f^2}TEC. \tag{3.17}$$

Practically, however, the geometric range cannot be measured and the TEC values are instead measured using the differential code delay and phase advance measurements on the L1 and L2 frequencies. Data is recorded by ground receivers in the Receiver INdependent EXchange (RINEX) format, with files containing the L1 and L2 carrier phase and pseudo path lengths for each satellite in view, either every 1 s or every 30 s. These ranges are calculated using a comparison of received and receiver generated signals and are thus biased by actual range, clock errors of receiver and satellite as well as instrumental bias and atmospheric effects (*Mannucci et al.*, 1996). The RINEX files also contain the pseudo ranges from the precise P code, P_1 and P_2, and the carrier phases,

L_1 and L_2. These can be expressed as in Equations 3.18 - 3.21 in terms of the ionosphere free pseudo range, P_0, which includes the geometric distance, tropospheric delays, clock errors and non-dispersive delays in the hardware signal paths, the integer ambiguity, a, the carrier wavelength, λ and the dispersive component of the receiver and satellite hardware errors, ϵ and τ as well as multipath errors (*Mannucci et al.*, 1996):

$$P_1 = P_0 + \frac{40.31TEC}{f_1^2} + \epsilon_1^r + \epsilon_1^s \tag{3.18}$$

$$P_2 = P_0 + \frac{40.31TEC}{f_2^2} + \epsilon_2^r + \epsilon_2^s \tag{3.19}$$

$$L_1 = P_0 - \frac{40.31TEC}{f_1^2} + a_1\lambda_1 + \tau_1^r + \tau_1^s \tag{3.20}$$

$$L_2 = P_0 - \frac{40.31TEC}{f_2^2} + a_2\lambda_2 + \tau_2^r + \tau_2^s. \tag{3.21}$$

Taking the difference between the phase and code range observables gives:

$$P_1 - P_2 = \frac{40.31TEC}{f_1^2 - f_2^2} + b_r + b_s \tag{3.22}$$

$$L_1 - L_2 = -\frac{40.31TEC}{f_1^2 - f_2^2} + a_1\lambda_1 - a_2\lambda_2 + b'_r + b'_s \tag{3.23}$$

where the the frequency-differenciated dispersive biases have been expressed as a single satellite or receiver bias term. Equation 3.22 allows us to obtain the TEC value along with a noise term, while Equation 3.23 gives the TEC with the associated integer ambiguity and interfrequency delay bias. This ambiguity remains constant while the satellite is visible. Absolute TEC can then be determined using a combination of Equations 3.22 and 3.23.

Due to the GPS satellite constellation configuration, the TEC measured is a slant TEC (STEC) and will depend on the location of the satellite. The VTEC, is the TEC directly above the receiver and is obtained from STEC through the use of a mapping function. For this mapping function, the ionosphere is assumed to be a thin shell at a height known as the effective height (EH), being the trasmitter-receiver ray intersection called the ionospheric pierce point

(IPP). This EH is assumed to be between 300 - 450 km. Using the geometry in Figure 3.1 gives:

$$STEC = \frac{VTEC}{\cos Z'}, \tag{3.24}$$

where Z' is the zenith angle of the satellite at the IPP. This can be written in terms of the satellite zenith angle Z at the receiver position using the relationship:

$$\frac{\sin Z}{R_E + H_{IPP}} = \frac{\sin Z'}{R_E}, \tag{3.25}$$

where R_E is the Earth's radius and H_{IPP} is the height of the IPP. VTEC measurements will be used in this study to identify disturbances of the ionosphere during geomagnetically quiet periods, predominantly over the African equatorial to midlatitude regions.

3.1.2 COSMIC

COSMIC comprises six satellites in 72° inclination orbits at an altitude of ~800 km, launched in April 2006 (*Pedatella and Larson*, 2010). The six COSMIC satellites are longitudinally evenly distributed and their daily rate of precession is ~12 min per day. Each satellite in the COSMIC array is equipped with a triband beacon, a small ionospheric photometer and four GPS antennae (*Pedatella and Larson*, 2010). Two of the GPS antennae are used for GPS radio occultation measurements and two are used for precise orbit determina-

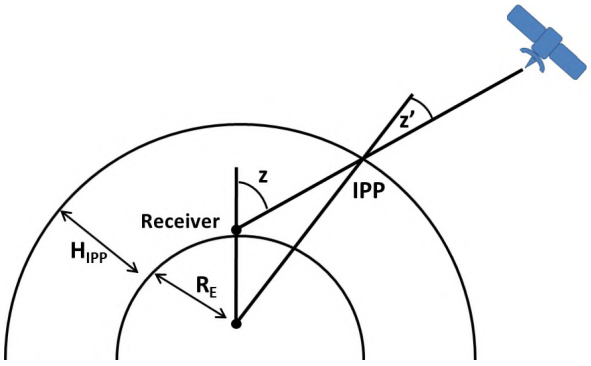

Figure 3.1: Schematic depiction of the geometry used in mapping STEC to VTEC. Figure adapted from *Hofmann-Wellenhof et al.* (1997).

tion (POD). This multi-instrument payload allows for the study of both the neutral atmosphere and the ionosphere.

3.1.2.1 PodTec

The primary purpose of the POD GPS antennae on each COSMIC satellite is to allow determination of satellite position with the precision and accuracy required to study GPS radio occultation. The POD and radio-occultation antennae also enable us to measure the TEC between GPS satellite altitude and the COSMIC satellites themselves. In a process identical to that used in calculating TEC between a GPS satellite and a ground station, the received GPS signals can be decoded and the carrier phase and pseudo range of both GPS frequencies can be derived, and these observations can be applied to calculated TEC data along the GPS ray between the COSMIC and GPS satellites.

COSMIC data is processed by the Cosmic Data analysis and Archive Center (CDAAC). TEC data is given by the COSMIC podTec dataset is generated by using the standard technique of levelling the ambiguous carrier-phase TEC to the absolute pseudo range TEC in order to generate a line of sight TEC between the COSMIC and GPS satellites. The podTec dataset thus comprises measurements of the POD antennae directed towards the GPS satellites wherein the absolute TEC along the ray path from each COSMIC satellite to each GPS satellite is recorded. Each podTec file contains continuous data from one GPS satellite with positions of the GPS and COSMIC satellites given every second together with the corresponding STEC measurement (*Yue et al.*, 2011).

Rays of positive elevation would measure TEC within the plasmasphere while rays with negative elevation correspond to TEC from below the horizon and give information about the E and F regions of the ionosphere (*Yue et al.*, 2011). Rays with negative elevation can be used to calculate the ionospheric TEC between the COSMIC satellite and a ground based GPS receiver. Rays

with positive elevation allow determination of the TEC between the COSMIC satellites at approximately 800 km and the GPS satellites at approximately 20 200 km altitude. Above 800 km the expected values of VTEC are usually less than 10 TECU, which means that small errors in the levelling bias are quite significant (*Pedatella and Larson*, 2010). The COSMIC POD observations are vulnerable to corruption by a significant multipath, which results in errors in the estimation bias. This multipath is thought to be due to the use of GPS antennae with poor multipath suppression as well as reflection of GPS signals off the solar panels. If carrier phase measurements are used in the plasmaspheric content then multipath is not a significant factor. The expected error from the CDAAC in these data is about 1-3 TECU for STEC (*Yue et al.*, 2011).

The absolute line-of-sight TEC observations in the podTec files must be converted to VTEC to allow comparison between the existing GPS VTEC data and the COSMIC TEC data. This conversion of STEC to the equivalent VTEC is usually done by representing the electron density distribution as lying within the ionosphere as a thick shell (e.g. *Sardon et al.* (1994)) or as a thin shell (e.g. *Lunt et al.* (1999b)). The thin shell conversion is given by Equation 3.26 where R_E is the radius of the earth, H_{IPP} is the effective altitude of the ionosphere and ζ is the elevation angle of the ray between the satellite and receiver.

$$VTEC = STEC \cdot \cos\left[\arcsin\left\{\frac{R_E}{R_E + H_{IPP}}\cos(\zeta)\right\}\right] \tag{3.26}$$

The thin shell conversion given in Equation 3.26 is the limit in zero thickness of the thick shell formula. An approximation of the thick shell formula, as given in Equation 3.27, can be used to accommodate for the electron density distribution of the ionosphere and plasmasphere, where ΔH is the effective thickness for the ionosphere and plasmasphere. This variant provides an approximation for the thick shell conversion for moderate effective thicknesses, allowing the effective altitude H_{IPP} to be retained for geographical calculations

of IPP locations.

$$VTEC = STEC \cdot \cos\left[\arcsin\left\{\frac{R_E}{R_E + H_{IPP} + \Delta H}\cos(\zeta)\right\}\right] \tag{3.27}$$

The expression given in Equation 3.27 can be used to convert the line of sight podTec TEC values to VTEC, as in *Mazzella* (2009). This differs from the geometric mapping function used by *Pedatella and Larson* (2010); *Yue et al.* (2011) and *Zhang et al.* (2017) to convert STEC to VTEC, which is based on the derivation by *Foelsche and Kirchengast* (2002).

Foelsche and Kirchengast (2002) note that for a plane parallel model of the Earth and the atmosphere, if the curvature of the Earth and the azimuthal variations within the atmosphere are neglected, the hydrostatic delay in an arbitrary slant direction ΔL_h can be written in terms of the elevation angle, ζ and the zenith hydrostatic delay, ΔL_h^0 as:

$$\Delta L_h = \mathrm{cosec}(\zeta)\Delta L_h^0. \tag{3.28}$$

More generally ΔL_h can be written in terms of a mapping function $m(\zeta)$ as:

$$\Delta L_h = m(\zeta)\Delta L_h^0. \tag{3.29}$$

The value of the mapping function can then be defined at the ratio of the slant straight-line ray path length within the 'effective height', S_{atm}, to the 'effective height', H_{atm}, itself as:

$$m(\zeta) = \frac{S_{atm}}{H_{atm}}. \tag{3.30}$$

This can then be written in terms of the cosecant law from Equation 3.28 as:

$$m(\zeta) = \frac{S_{atm}}{\sin(\zeta)\dot{S}_{flat}}, \tag{3.31}$$

with S_{flat} as the ray path within H_{atm} in a flat atmosphere. Using the geometry shown in Figure 3.2, S_{atm} can be determined using the triangle formed by R_E, $R_E + H_{atm}$ and S_{atm}. The ratio $\tilde{r}$ can then be introduced as:

$$\tilde{r} = \frac{R_E}{R_E + H_{atm}}, \tag{3.32}$$

to write S_{atm} as:

$$S_{atm} = (R_E + H_{atm}) \left[\cos\left(\arcsin(\tilde{r}\cos\zeta)\right) - \tilde{r} sin\zeta\right], \tag{3.33}$$

and therefore obtain the final form of the mapping function as:

$$m(\zeta) = \left(\frac{R_E}{H_{atm}} + 1\right) \left[\cos\left(\arcsin(\tilde{r}\cos\zeta)\right) - \tilde{r}\sin\zeta\right]. \tag{3.34}$$

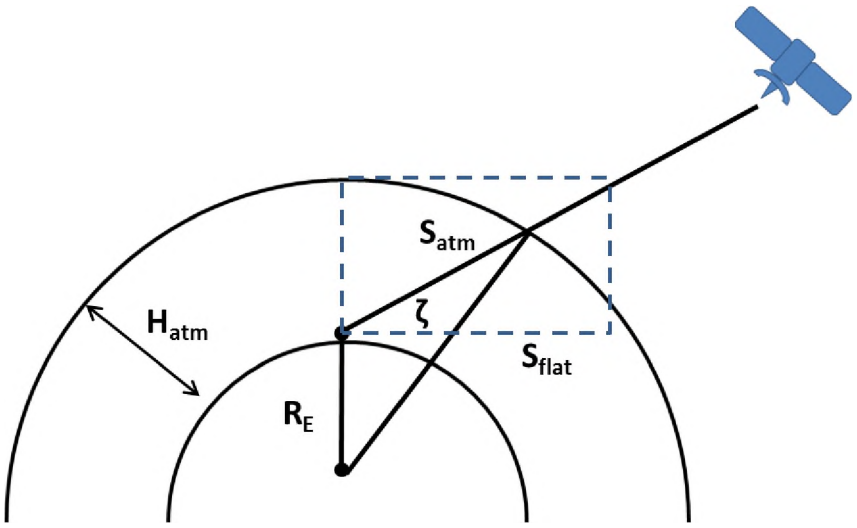

Figure 3.2: Schematic depiction of the mapping function used to convert STEC to VTEC for the plasmasphere. Figure adapted from *Foelsche and Kirchengast* (2002).

Since the role of hydrostatic delay in an arbitrary slant direction is taken in our problem by STEC and the zenith hydrostatic delay is VTEC, STEC

can be converted to VTEC using:

$$VTEC = STEC \left[\left(\frac{R_E}{H_{atm}} + 1 \right) \{ \cos\left(\arcsin(\tilde{r} \cos\zeta) \right) - \tilde{r} \sin\zeta \} \right]^{-1}. \quad (3.35)$$

The plasmaspheric contribution to TEC is large during the period under study, rendering the thin shell approximation (given by Equation 3.26) a poor representation of atmospheric electron density. Although the thick shell approximation (given by Equation 3.27) can be used to compensate for a large plasmaspheric contribution, the precedent set in *Pedatella and Larson* (2010), *Yue et al.* (2011) and *Zhang et al.* (2017) will be followed and the plasmaspheric VTEC will be calculated using Equation 3.35 in this study.

3.1.3 Magnetometer

The strength and fluctuations of the Earth's magnetic field are measured using a magnetometer. The most common magnetometer types are fluxgate, liquid and vapour, which measure the parameters illustrated in Figure 3.3. These parameters are:

- X is the North-South component of the magnetic field, defined to be positive northwards and measured in nT,
- Y is the East-West component of the magnetic field, defined to be positive

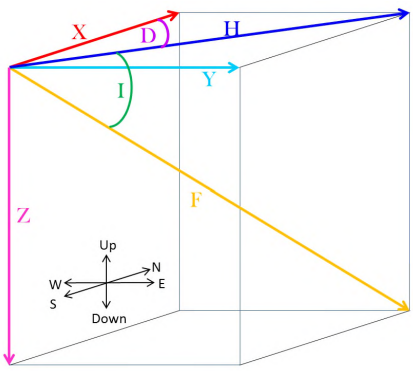

Figure 3.3: Schematic depiction of the components of the Earth's magnetic field. Figure adapted from http://www.intermagnet.org/faqs-eng.php#geomagnetic-comp.

eastwards and measured in nT,

- Z is the vertical component of the magnetic field, defined to be positive downwards and measured in nT,
- F is the total intensity of the magnetic field, measured in nT,
- D is the magnetic declination, i.e. the angle between true North and magnetic North, defined to be positive eastwards of true North and measured in degrees,
- I is the magnetic inclination. I is defined to be the angle between the horizontal plane and the total field vector, F, measured in degrees, and
- H is the horizontal intensity of the magnetic field vector, measured in nT.

The Earth's magnetic field is a vector quantity and can be completely described by the three orthogonal strength components, X, Y and Z, or by the total field strength, F, and two angles, D and I, or by two strength components, H and Z, and an angle, D. These parameters can be related through Equations 3.36-3.41 below:

$$F = \sqrt{X^2 + Y^2 + Z^2} \tag{3.36}$$

$$D = arctan\left(\frac{Y}{X}\right) \tag{3.37}$$

$$I = arctan\left(\frac{Z}{H}\right) \tag{3.38}$$

$$H = \sqrt{X^2 + Y^2} \tag{3.39}$$

$$X = H\cos(D) \tag{3.40}$$

$$Y = H\sin(D). \tag{3.41}$$

Indices used as indicators of geomagnetic activity, including geomagnetic storms and substorms are calculated from the abovementioned parameters, measured by magnetometers located at geomagnetic observatory stations across the Earth.

3.1.3.1 Dst Index

Periods of great magnetic disturbance result in depression of the horizontal component of the geomagnetic field, H. The decrease in H during a magnetic storm can be represented by a southward directed, uniform magnetic field parallel to the geomagnetic dipole axis in the equatorial and midlatitude regions. The disturbance storm time (Dst) index is defined to represent this disturbance of the H component, and is regarded as a function of storm time. Dst is derived using four magnetic observatories, which are distant from both the auroral and equatorial electrojets and are longitudinally approximately evenly distributed (*Sugiura and Kamei*, 1991). These four observatories are Hermanus, Kakioka, Honolulu, and San Juan. Figure 3.4a presents the variation of the Dst index for days 200-210 of 2009, which shows a geomagnetic disturbance recorded on day 203. The Dst index is used in this study to classify whether a disturbance of the ionosphere occurs under quiet or disturbed geomagnetic conditions.

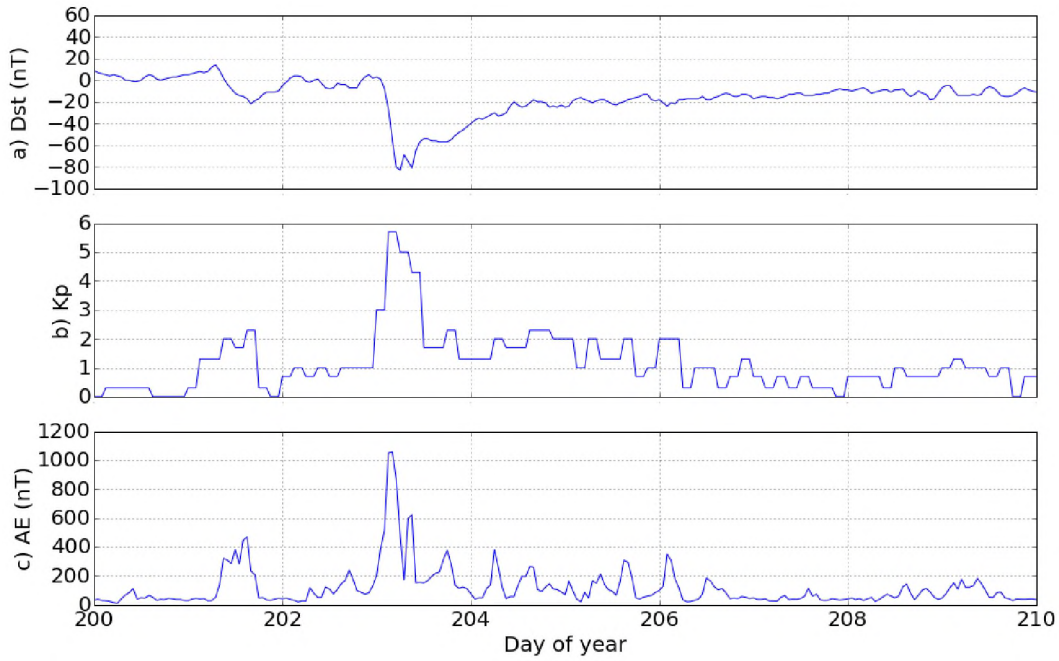

Figure 3.4: A plot of the temporal variation of the geomagnetic indices, a) Dst, b) Kp and c) AE, for days 200-210 of 2009.

3.1.3.2 Kp Index

The K index is a three-hourly index derived using the maximum fluctuation of the H component at any particular observatory. It provides the state of the geomagnetic field at the location of the observatory. The planetary K index (Kp) provides a global geomagnetic storm index and is derived from the K indices measured at 13 selected subauroral stations, as described in *Bartels and Veldkamp* (1949). The K and Kp indices vary between 0-9, with the following designations of the magnetic condition.

- 0-3: Quiet
- 3-6: Moderately disturbed
- 6-9: Strongly disturbed

Figure 3.4b shows the variation of the Kp index from day 200-210 of 2009, showing the disturbance of Kp during the geomagnetic storm commencing on day 203. The Kp index will be used as the second indicator of whether an ionospheric disturbance occurs under quiet or disturbed geomagnetic conditions.

3.1.3.3 AE Index

The Auroral Electrojet (AE) index provides a measure of substorm activity in the Earth's magnetic field and represents the overall activity of the electrojets. The AE index is derived from variations of the H component as observed at selected observatories in the auroral zone of the northern hemisphere (*Davis and Sugiura*, 1966). In order to calculate the AE index, first the data must be normalised. A monthly base value of the H component is calculated for each station by averaging the data for the station on the five international quietest days (*Davis and Sugiura*, 1966). This base value is then subtracted from the one minute data for that station. The upper and lower envelopes of the data are then determined by selecting the largest and smallest values for

all the stations at each given time. These values form the AU and AL indices, respectively, which represent the strongest current intensity of the eastward and westward electrojets, respectively. The AE index is then calculated as the difference of the AU and AL indices, as shown in Equation 3.42.

$$AE = AU - AL \tag{3.42}$$

Figure 3.4c shows the variation of the AE index from day 200-210 of 2009, showing the geomagnetic storm on day 203 as well as a number of substorm events on days 204-206. In this study, the AE index will be used to investigate the role of substorm activity in the formation of Q-disturbances of the ionosphere.

3.2 Data Analysis

3.2.1 Q-disturbances

Data from 10 GPS stations over the African latitudes for 2009 (during solar minimum) and 2013 (near solar maximum) were analysed. Table 3.1 presents the geographic and geomagnetic co-ordinates of these stations. Four of these GPS stations lie in the equatorial region, of which two are situated within the equatorial trough. Two lie close to the crest of the equatorial ionisation anomaly. The remaining six stations are located in the southern midlatitude region. The location of the stations are shown in Figure 3.5.

A GPS-TEC software developed at Boston College (*Seemala and Valladares*, 2011) was used to derive TEC measurements from dual-frequency GPS observations. Effects of non-frequency dependent terms (such as range, satellite and reciever clock errors and tropospheric delay) in the calculation of STEC are eliminated through the use of code and phase values for L1 and L2 frequencies (f_{L1} = 1 575.42 MHz and f_{L2} = 1 227.60 MHz) within this

Table 3.1: Geographic and geomagnetic longitude and latitude of the GPS stations used. Geomagnetic coordinates obtained from: http://www.ukssdc.ac.uk/cgi-bin/wdcc1/coordcnv.pl.

Latitudinal Region	Station ID	Geographic		Geomagnetic	
		latitude	longitude	latitude	longitude
Equatorial trough	NAZR	8.568	39.29	-0.25	111.01
	ROBE	7.113	40.026	-1.69	111.78
Equatorial crest	MBAR	-0.601	30.738	-10.22	102.36
	MAL2	-2.996	40.194	-12.42	111.86
Midlatitude	WIND	-22.575	17.089	-33.16	84.64
	SPRT	-24.671	30.185	-35.25	97.71
	EMLO	-26.498	29.984	-36.81	96.80
	SBOK	-29.669	17.879	-39.03	82.85
	DRBN	-29.850	31.023	-39.49	96.39
	HNUS	-34.425	19.223	–42.35	82.15

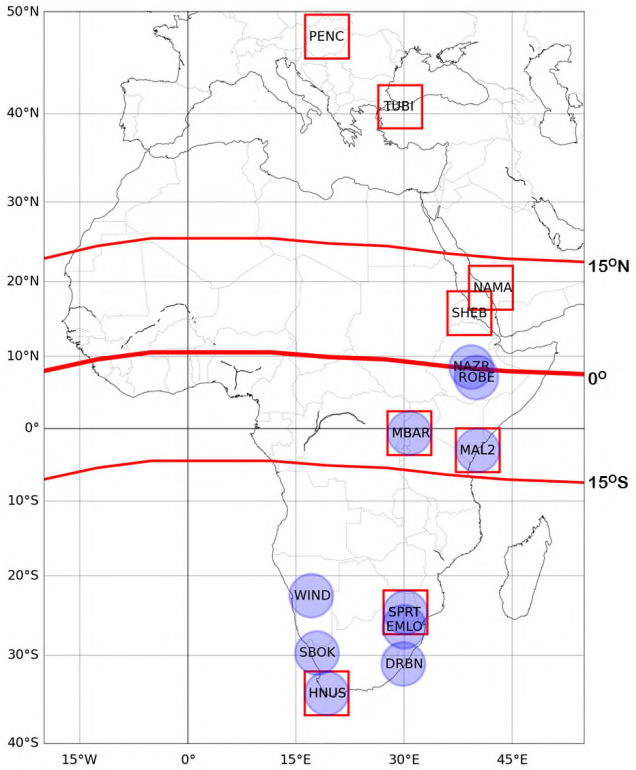

Figure 3.5: Map of GPS stations (observation points). The red lines denote the geomagnetic latitude, with the midlatitude stations lying below 15°, the equatorial trough stations lying on the geomagnetic equator (0°) and the equatorial crest stations lying between 0-15°S. Stations marked by blue circles were used in determining the morphology of Q-disturbances over Africa. Stations marked by red squares were used in analysing the relationship between conjugate stations.

software. In order to give absolute TEC measurements, the software uses differential satellite biases published by the University of Bern and receiver biases calculated by minimising the TEC variability between 02:00 and 06:00 LT (local time) (*Seemala and Valladares*, 2011). The STEC value is then used to derive the VTEC value, assuming a thin shell ionosphere at 350 km.

In this study, VTEC values, measured in TECU (10^{16} electrons m^{-2}), were calculated from satellites above 35° elevation in order to mitigate multi-path effects. Variations from a 27 day running median were used to calculate dVTEC as in Equation 3.43. The day to day variation of VTEC is $\sim \pm 45\%$ (*Matamba et al.*, 2015), thus dVTEC $\geq$45% or dVTEC$\leq$-45% are considered significant. In order to minimise noise in the data, variations in dVTEC were considered to be an enhancement (depletion) only if dVTEC remained greater (less) than 45%(-45%) for at least 30 minutes. Enhancements (depletions) separated by less than 30 minutes were considered to be part of the same event.

$$dVTEC = \frac{VTEC_{observed} - VTEC_{median}}{VTEC_{median}} \tag{3.43}$$

The main interest of this thesis lies in disturbances not related to disturbances of the geomagnetic condition. The Dst and Kp indices are used as the indicators of magnetic disturbance intensity and development, where the day was considered to be quiet if Dst $\geq$ -30 nT and Kp $\leq$ 2 (*Mikhailov et al.*, 2007). All dVTEC disturbances commencing within a period of 24 hours subsequent to a geomagnetic disturbance were excluded to eliminate effects on the ionosphere from geomagnetic variations (*Mikhailov and Perrone*, 2009).

A disturbance was considered to be a daytime event if that disturbance commenced between local sunrise and ten minutes after local sunset on the ground. Local sunrise/sunset was obtained for individual stations for the days of disturbance from www.timeanddate.com and www.sunrise-and-sunset.com. All other disturbances were considered to be nighttime events and are further split into pre- and post-midnight events. Data gaps exist due to operational

downtimes and corrupt data. Only stations with $\geq 65\%$ data available per year were included in the analyses. The resulting morphology of Q-disturbances is discussed in Chapter 4, as well as the implications of the observed morphology on mechanisms suggested in literature.

3.2.2 Plasmaspheric Contribution to TEC

TEC is derived by measuring the difference in delay between dual-frequency signals transmitted from the GPS satellites to ground receivers. The ray path between a GPS station and the GPS satellite travels through both the plasmasphere and the ionosphere. It is along this ray path that the TEC is measured. The majority of the electron content along this ray path is expected to lie within the F2-layer of the ionosphere and calculations of TEC typically assume that this thin layer is the dominant component and that the contribution from the plasmasphere can be neglected. However, it has been shown that although the absolute value of the TEC within the plasmasphere is low, this region has a significant contribution under certain conditions. In particular, *Balan et al.* (2002); *Lunt et al.* (1999a) and *Yizengaw et al.* (2008) found that the plasmaspheric portion of nighttime TEC can be up to 50% at solar minimum during winter.

Experimental measurements of protonospheric electron content can be made by using data from low earth orbit (LEO) satellites such as the Navy Ionospheric Monitoring System (NIMS), the Challenging Mini-Satellite Payload (CHAMP) or COSMIC. The difference of GPS pseudorange and carrier phase measurements in two frequencies gathered by the GPS zenith-oriented antenna, connected to the GPS receiver on-board the LEO satellite, can provide a measure of the electron content on the plasmaspheric portion of the GPS ray paths. Absolute ionospheric TEC can then be found by removing the plasmaspheric contribution from the GPS TEC measurement, after estimating and removing the pseudorange DCBs and carrier phase ambiguities. In particular, data from

the COSMIC array will be used as these satellites have good data coverage for the period of interest. Although the ionospheric TEC can be determined more directly through the use of podTEC data with negative elevation angles to measure TEC directly between the COSMIC satellite and a GPS ground station, there is a substantially smaller number of data points available. This implies a better determination of the plasmaspheric contribution to the ionospheric TEC measured directly between the GPS satellite and ground receiver can be obtained by using podTEC data with positive elevation angles and removing the plasmaspheric TEC directly from the measured ionospheric TEC.

In order to assess the contribution of the plasmasphere to the measured TEC, an analysis of the plasmaspheric contribution was undertaken. As the contribution of the plasmasphere is expected to be most significant during solar minimum and at night in the midlatitude region, data from 2009 will be used for this analysis. The effects are expected to be significant over the midlatitude region, so this region will be the focus of this analysis. In addition, the midlatitude stations from the conjugate station analysis will be used so that the results over this region and the contribution of the plasmasphere may be consistently compared and discussed. A further analysis of the occurrence of Q-disturbances at conjugate stations, with the plasmaspheric contribution removed, was done. For this reason, the stations selected were HNUS, SPRT, TUBI and PENC, as illustrated in by the red squares in the midlatitude regions of Figure 3.5.

In order to analyse the plasmaspheric contribution, the first step is to define the region of sky in which a satellite gives data relevant to the station of interest. The location of the COSMIC satellites is defined through the use of the concept of a plasmaspheric penetration point (PPP). This is defined as a parallel to the IPP, which means it is the point at which the ray path pierces the plasmasphere. Since the average altitude of the COSMIC orbit is at 800 km, this height is used to define the PPP and H_{PPP} is used as 800km. For an

elevation angle ζ, the COSMIC satellite must lie within the region defined by the PPPs, as illustrated in Figure 3.6, for the station SPRT.

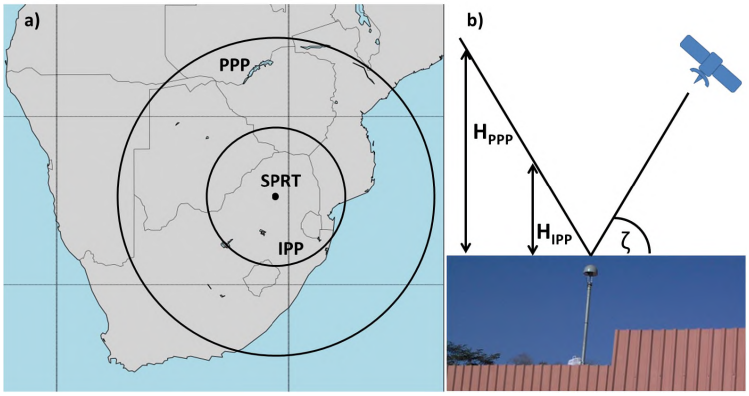

Figure 3.6:
a) Concentric rings represent the IPP and PPP around the SPRT receiver. b) The IPP and PPP are defined by the minimum elevation angle ϵ from the GPS receiver to the satellite at the IPP and PPP heights. Image of SPRT receiver taken from http://www.trignet.co.za/Map/SensorMap.aspx.

The podTec values will be used to calculate the plasmaspheric portion of the TEC, so only positive elevation angles are of interest. In addition, multipath effects are a major factor for the COSMIC TEC measurements, so the elevation angle must be considered carefully (*Pedatella and Larson*, 2010). In order to avoid multipath effects and remain within the region studied in the GPS TEC observations, a minimum elevation of 35° will be used for the elevation angle between each COSMIC-GPS pair of satellites. The region of allowed COSMIC positions is thus defined by the PPP at 35°. This gives a circular region with a radius of 1 143 km centred on the station of interest.

Once the PodTec data for the appropriate region has been extracted, the line of sight TEC or STEC must be converted into VTEC. Equation 3.35 is used to convert the COSMIC podTec STEC measurements to VTEC measurements, following the precedent set in *Pedatella and Larson* (2010), *Yue et al.* (2011) and *Zhang et al.* (2017). As in *Yue et al.* (2011); *Zhang et al.* (2017), the value of H_{atm} has been taken to be 3 000 km. The resulting $VTEC_{plasma}$ data has a low resolution with satellite passes occurring approximately every hour.

Median hourly values were thus calculated for both the GPS data obtained from Equation 3.43, $VTEC_{GPS-hr}$, and the COSMIC data, $VTEC_{plasma-hr}$. The ionospheric component of $VTEC_{GPS-hr}$ was then calculated by:

$$VTEC_{iono} = VTEC_{GPS-hr} - VTEC_{plasma-hr}. \tag{3.44}$$

Deviation from a 27 day running median was then calculated for each Q-disturbance at each station using

$$dVTEC_{iono} = \frac{VTEC_{iono} - VTEC_{iono-median}}{VTEC_{iono-median}}. \tag{3.45}$$

A 27-day running median is used to eliminate errors for disturbances occurring at the beginning or end of a month. These new $dVTEC_{iono}$ values were then analysed through comparison with the GPS dVTEC obtained from Equation 3.43, to determine the contribution of the plasmasphere to the size and occurrence of Q-disturbances. The conjugate stations were also analysed to give further insight as to whether there exists a relationship between the occurrence of Q-disturbances at conjugate stations when the contribution of the plasmasphere is accounted for. These results will be discussed in Section 5.2

3.3 Summary

GPS can be used to measure TEC, which is then used to study the variability of the ionosphere. GPS TEC data will be used to study Q-disturbances of the ionosphere primarily over the African region. In addition, TEC from COSMIC will be used to determine the contribution of the plasmasphere to GPS TEC and thus to explore the role of the plasmasphere in Q-disturbance formation. The Kp and Dst indices, derived from magnetometer data, will be used to ensure that the ionospheric disturbances studied occur under quiet geomagnetic conditions. The AE index will be used to analyse the influence of substorm activity on Q-disturbance occurrence.

Chapter 4

Morphology of Q-disturbances over African Latitudes

One of the primary goals of this thesis is to characterise the morphology of Q-disturbances of the ionosphere over African latitudes. An analysis of these disturbances has been undertaken using the procedure described in Section 3.2.1.

An example of Q-disturbances observed at the EMLO GPS station during September-October 2009, is shown in Figure 4.1. Specifically, enhancements are seen on days 267, 274, 276, 281 and 286, whilst depletions are seen on days 275, 280 and 283. Enhancements/depletions on days 262-265, 271, 277, 284 and 285 were excluded as Q-disturbances due to several reasons, such as Kp values larger than the defined threshold, duration of enhancement being less than the defined threshold and/or poor data quality. Many Q-disturbances were observed in the data set over Africa and these have been analysed to explore the variation of the observed occurrences, duration and intensity of Q-disturbances per latitude region, time of commencement, solar cycle and season.

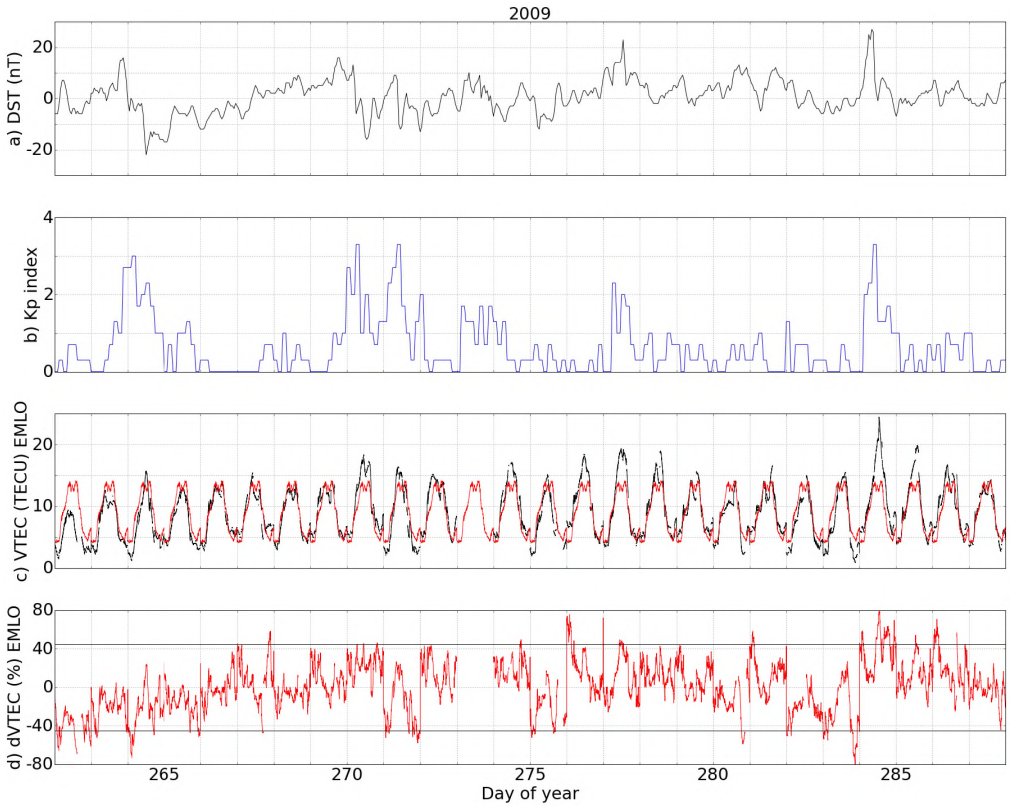

Figure 4.1: Behaviour of VTEC at the Ermelo (EMLO) GPS station during September-October 2009 showing a) Dst and b) Kp indices as well as c) the local VTEC and 27-day running median VTEC and d) percentage deviation from median of the VTEC.

4.1 Total Number of Q-disturbances

The total number of Q-disturbances observed over the different latitudinal sectors of Africa during solar maximum (2013) and solar minimum (2009) as a median of the total number of events per station is illustrated in Figure 4.2 for each region, respectively. The number of daytime, pre- and post-midnight events are stacked to reach the total median number of events per station per region. Data gaps were compensated for by weighting data for each station according to the amount of data available.

In general, daytime Q-disturbances (i.e. enhancements and depletions) are seen less frequently than nighttime Q-disturbances, as shown in Figure 4.2. Enhancements occur most frequently in the pre-midnight sector, while depletions are more frequently observed during the post-midnight sector.

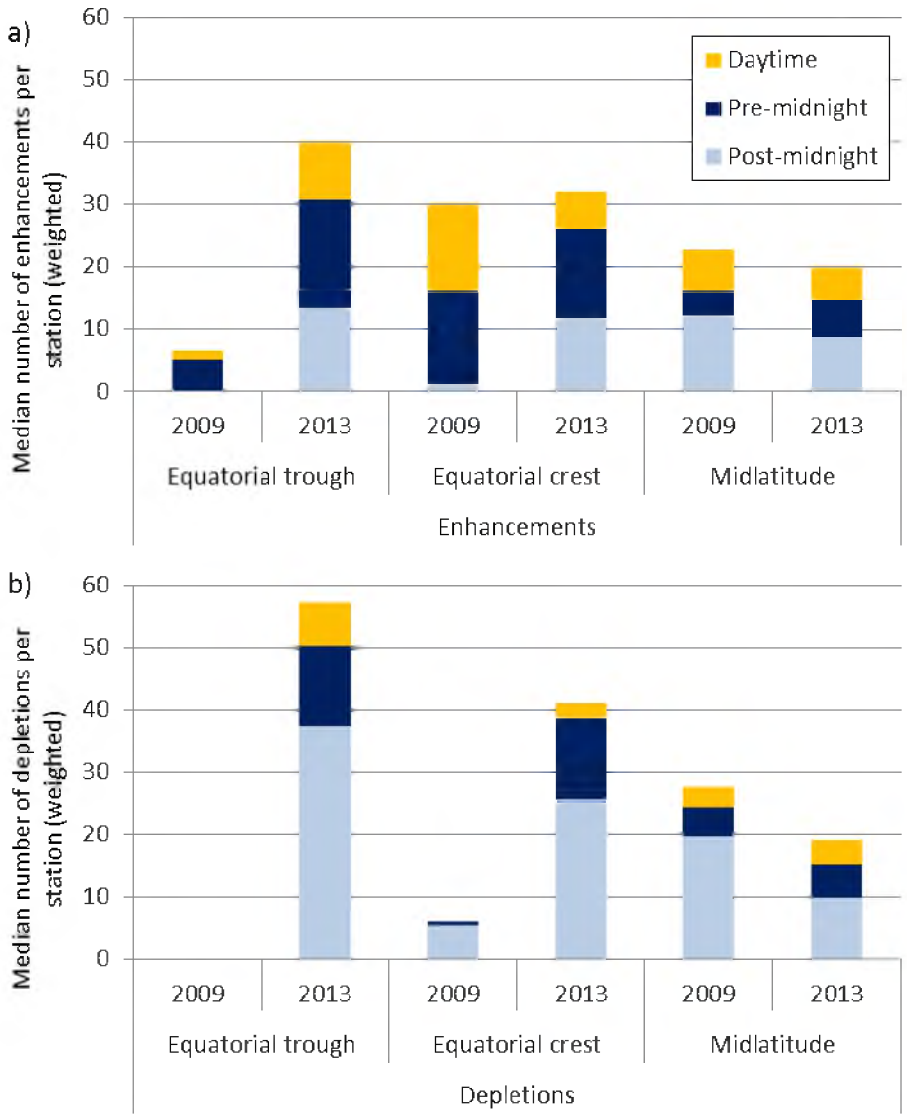

Figure 4.2: Median number of a) Enhancements and b) Depletions commencing during daytime, pre- and post-midnight, stacked to show the total median number of Q-disturbances observed per station for each latitudinal region in Africa, during solar minimum (2009) and solar maximum (2013).

In general depletions are seen more than enhancements, except during solar minimum in the equatorial regions, where enhancements are more frequently seen. However, daytime enhancements are more common than daytime depletions.

A higher number of Q-disturbances is seen during solar maximum in the equatorial regions, with the difference in frequency of occurrence most pronounced for depletions. In the midlatitude region, the difference in total occurrence of disturbances between solar minimum and maximum is much smaller than in the equatorial regions, however more Q-disturbances are observed during solar minimum in this region.

The monthly occurrence of Q-disturbances for different times of commencement is illustrated in Figure 4.3. The number of depletions in the equatorial trough region as well as the number of daytime and pre-midnight depletions during solar minimum are too small to show any trends in seasonal behaviour and have thus been excluded from discussion of seasonal trends. These results indicate that there is no systematic or simple seasonal trend across latitudinal regions.

For example, in the midlatitude region the largest number of daytime Q-disturbances occur during the equinoxes, except for depletions during solar minimum where a slightly higher number of winter disturbances are seen. In the equatorial crest region, daytime enhancements are seen most often in the winter and least often in the summer, while for depletions during solar maximum, this observation reverses. However, daytime enhancements in the equatorial trough are most frequent in winter only during solar minimum, while they are most frequent at the equinoxes during solar maximum. Furthermore, daytime depletions are most frequent during summer and least often observed during the winter months.

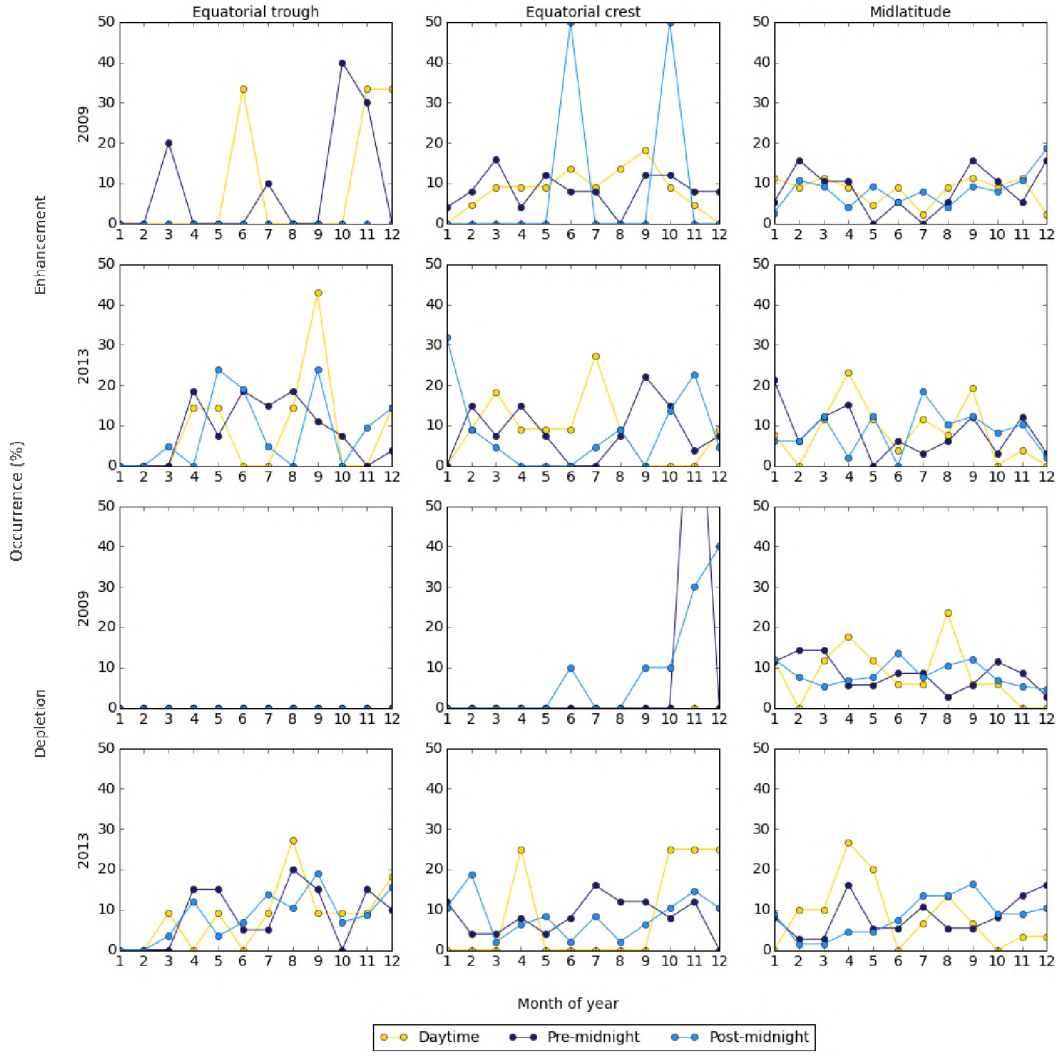

Figure 4.3: Number of Q-disturbances per region as a percentage occurrence per month.

4.2 Duration of Q-disturbances

The probability mass distribution of the duration of occurrence of Q-disturbances for daytime, pre- and post-midnight in different latitudinal regions using a bin width of 2 hours is shown in Figure 4.4. The daytime, pre- and post-midnight duration occurrences are stacked to show the total probability of a duration occurring in a specific bin for a given time of day.

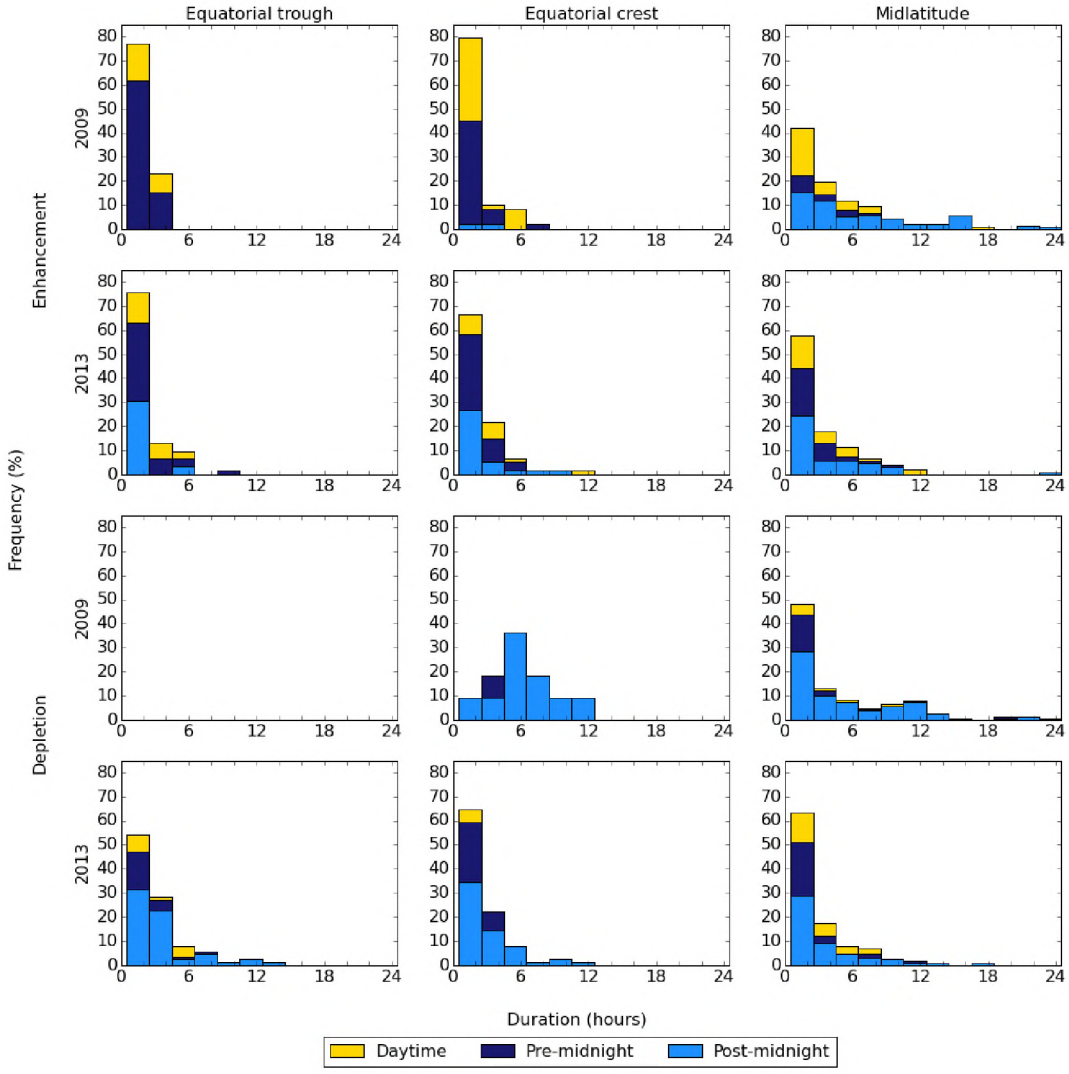

Figure 4.4: Duration of Q-disturbances (Daytime, pre- and post-midnight events are shown as fractional contribution towards overall occurrence probability).

In general, the most frequent duration of Q-disturbances is 0.5 - 2.5 hours, except for post-midnight depletions in the equatorial crest region during solar minimum, which are more likely to be 4.5-6.5 hours long. Long duration events (>12 hours) are only seen in the midlatitude region and are seen for both enhancements and depletions; with the largest number of long duration events occurring during solar minimum. Q-disturbances in the equatorial crest region are also more likely to last longer than 4.5 hours than those in the equatorial trough.

4.3 Q-disturbance Amplitude

The amplitudinal variation of VTEC Q-disturbances in the three different latitudinal regions of interest is illustrated in Figure 4.5 and is shown as the probability mass distribution of the maximum dVTEC (%) seen in each region and for each time sector using a bin width of 10%. The graph has been plotted such that the probabilities of day, pre- and post-midnight are stacked to give the total probability of dVTEC falling in that bin for a given time of day.

The frequency of occurrence of disturbances of various sizes is complex. Overall, more large enhancements are seen than large depletions. The number of large enhancements increases as latitude increases during solar minimum. Large Q-disturbances (i.e. dVTEC $\geq$ 65%) are seen more frequently during solar maximum than during solar minimum. Very large depletions (i.e dVTEC $\geq$ 85%) are generally only seen during solar maximum with the largest depletions seen in the midlatitude region.

In the midlatitude region, Q-disturbances are generally more likely to have amplitudes of 45-55% and this trend is seen for daytime and pre-midnight events. Post-midnight disturbances at solar maximum have a similar trend, while post-midnight enhancements at solar minimum have the highest proba-

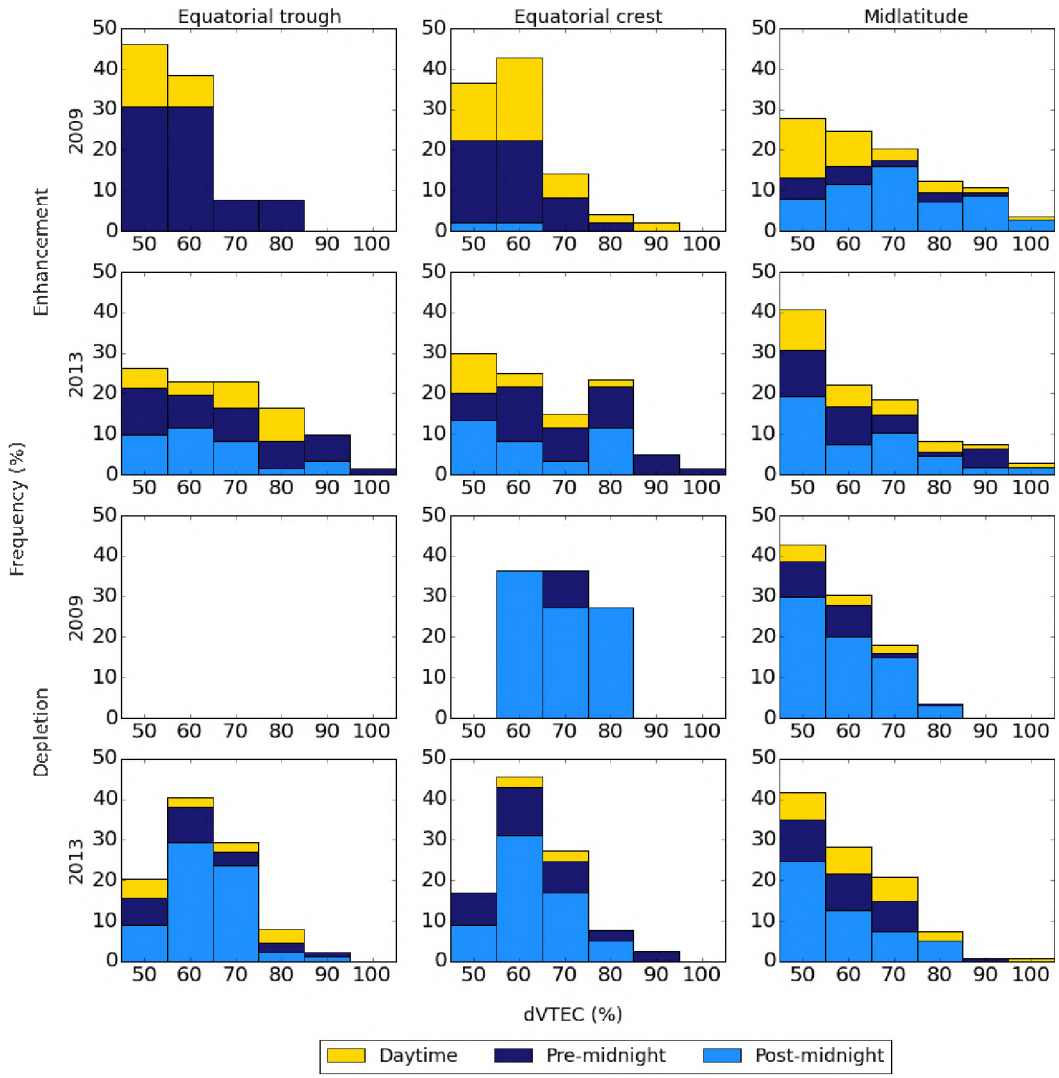

Figure 4.5: Maximum dVTEC for Q-disturbances in each latitude region for events commencing in daytime, pre- and post-midnight.

bility of having amplitudes of 65-75%.

In the equatorial crest region, the size of enhancements and depletions differs between solar minimum and solar maximum. Enhancements are typically marginally larger during solar minimum (55-65%) with pre- and post-midnight events falling with equal frequency between 45-65%. During solar maximum, equatorial crest enhancements are most likely to be 45-55% overall as well as for daytime and post-midnight events, while pre-midnight events are often larger (55-65%). Equatorial crest depletions during solar minimum are most frequently 55-75% with post-midnight events (55-65%) marginally smaller than pre-midnight events (65-75%). Depletions in the equatorial crest during solar maximum are overall predominantly 55-65% with the same dominance of occurrence for pre- and post-midnight events, while daytime depletions are likely to be 55-75%.

In the equatorial trough region enhancements are most likely to be 45-55%, with this trend mirrored by daytime enhancements and pre-midnight events during solar maximum. However, pre-midnight enhancements in this region during solar minimum are equally likely to be 45-65%. Post-midnight Q-disturbances during solar maximum are dominantly 55-65%. Overall during solar maximum, depletions are most likely to be 55-65% with daytime depletions being smaller at 45-55%.

4.4 Discussion

In this study, it is noted that nighttime Q-disturbances are seen most often over the African locations analysed. The less frequently seen daytime Q-disturbances are more often enhancements than depletions. The results also show that short-term disturbances (<3 hours) are most frequent but long duration Q-disturbances (>12 hours) are typically only seen during solar minimum. In addition, the size of depletions is strongly dependent on local time

and solar activity, with larger events occurring during the night and at solar minimum, while enhancements have a more moderate dependence on these conditions. These results agree with those noted in *Depueva et al.* (2005).

While this study found depletions to be more numerous than enhancements in the equatorial region over Africa during solar maximum, *Depueva et al.* (2005) found this to hold true throughout the solar cycle. In addition, this study reveals no seasonal trend for the African equatorial region, which agrees with the trend over Kodaikanal but differs from the seasonal trend over Huancayo, which are discussed in *Depueva et al.* (2005). *Depuev et al.* (2008) and *Depueva et al.* (2005) suggested $\mathbf{E}\times\mathbf{B}$ vertical drift as the major source for Q-disturbances in the equatorial region and this matches well with the morphology observed in this study over the African region.

In the equatorial region, variations of the F2-layer are predominantly controlled by variations in $\mathbf{E}\times\mathbf{B}$ vertical plasma drifts with minimal contributions from thermospheric winds as the magnetic inclination, $I = 0$ at the geomagnetic equator (*Depueva et al.*, 2005). This vertical drift is directed downward during the night, lowering hmF2, which in turn results in a higher recombination rate. Q-disturbances in this region are caused by recombination of $[O^+]$ ions, which represent the main ion in the F2 region (*Depueva et al.*, 2005). This mechanism results in large numbers of depletions observed during the nighttime and can explain the dominance of nighttime Q-disturbances observed in the equatorial regions in this study.

Nighttime vertical $\mathbf{E}\times\mathbf{B}$ has a systematically smaller amplitude during solar minimum than during solar maximum with large day to day variability (*Fejer et al.*, 1991). This implies that while vertical $\mathbf{E}\times\mathbf{B}$ is usually small at solar minimum, large negative vertical $\mathbf{E}\times\mathbf{B}$ can occur. However, at solar maximum, the nighttime vertical $\mathbf{E}\times\mathbf{B}$ is usually moderate and negative. In addition, the thermospheric temperature is higher at solar maximum, result-

ing in larger differences between the neutral scale heights of $[N_2]$ and $[O_2]$ at solar maximum than during solar minimum (*Hedin*, 1987). This means that a shift of the F2 layer height by the same amount would give larger changes in the recombination rate during solar minimum when the neutral scale height difference is smaller. This results in a higher frequency of occurrence of depletions at solar maximum, which agrees with the results presented in Figure 4.2, while depletions at solar minimum are more likely to have large amplitude and long duration, which is in agreement with the observations presented in Figures 4.4 and 4.5. In addition, average $\mathbf{E}\times\mathbf{B}$ drift is large and negative during the post-midnight sector during solar minimum (*Fejer et al.*, 1991), implying that conditions are more favourable for depletions during the post-midnight sector. In other words, post-midnight depletions occur more frequently than pre-midnight depletions, as observed in this study.

Another contributing factor in the equatorial region is the large pre-reversal upsurge of vertical drift during post-sunset hours at solar maximum, which is seldom seen during solar minimum (*Fejer et al.*, 1991). This upsurge lifts plasma into the topside ionosphere where it is stored in the magnetic tubes of force. Any nighttime increase of the vertical drift hereafter will therefore be accompanied by an influx of plasma, largely compensating for recombination losses. Thus more pre-midnight enhancements than depletions may be observed at solar maximum in the equatorial crest region, which is illustrated by the results presented in Figure 4.2.

The magnetic tubes of force are small in the equatorial region and the plasma content is thus small. This means the process will only be effective for the early hours of the night, after which the magnetic tubes of force will no longer result in an influx of ions and the recombination losses will dominate during the later hours of the night, resulting in negative Q-disturbances during the post-midnight hours. Therefore more post-midnight depletions than enhancements would be expected in the equatorial regions during solar max-

imum, which is shown in Figure 4.2. During solar minimum however, this effect is infrequent, resulting in disturbances that may start earlier in the night and last longer. This expected behaviour agrees with the occurrence of Q-disturbances observed in this study over the equatorial latitudes.

Depueva et al. (2005) observed a seasonal trend in Huancayo but no significant seasonal behaviour in Kodaikanal. As both stations are located in the equatorial latitudes but at different longitudes, *Depueva et al.* (2005) therefore postulated the existence of a non-seasonal component of $\mathbf{E}\times\mathbf{B}$, as well as a seasonal component, with the seasonal component forming a standing planetary wave to explain the different seasonal trends at the two stations. Within this postulate, Kodaikanal would then need to lie at a minima of this standing wave with Huancayo lying at a point where the seasonal standing wave has a significant contribution. In this study, the behaviour of the equatorial Q-disturbances show no significant seasonal variation, suggesting that the African region could correspond to an additional minimum of the above-mentioned seasonal standing planetary wave, or there could be an additional factor contributing to seasonal variation over Huancayo that does not exist over Kodaikanal and the Africa equatorial region.

In the midlatitude region in this study, daytime Q-disturbances were comparatively rare with the majority of events occurring in the post-midnight sector. A larger number of events occur during solar minimum than during solar maximum. Events in the midlatitude region were found to be mostly of short duration with long events more frequent at solar minimum. The above-mentioned observations of this study for the midlatitude region are similar to the results found by *Farelo et al.* (2002) and *Mikhailov et al.* (2004).

Seasonal behaviour over the African midlatitude region differs distinctly from the studies by *Farelo et al.* (2002) and *Mikhailov et al.* (2004). In this study, the data shows no clear seasonal trend for enhancements or depletions

at any time of day. *Farelo et al.* (2002) and *Mikhailov et al.* (2004), however found Q-disturbances to show seasonal variations in occurrence with depletions seen most frequently in winter, daytime enhancements occurring around the equinoxes and nighttime enhancements having no pronounced variation.

The mechanism behind Q-disturbances in the midlatitude region is not as easy to isolate as the equatorial region and a number of mechanisms have been suggested to contribute to the observed morphology. Possible mechanisms suggested by *Mikhailov et al.* (2004) include neutral composition, plasmaspheric fluxes, thermospheric winds, solar EUV radiation variations, while *Farelo et al.* (2002) suggested the above mechanisms as well as plasmaspheric transfer from conjugate points and direct solar photoionisation. These mechanisms are all thought to play a role in the formation of Q-disturbances at midlatitudes and the influence of each mechanism varies with geophysical conditions.

In this study, positive nighttime Q-disturbances with the largest amplitudes are found at midlatitudes during solar maximum in summer. In the midlatitude region, there is a decrease in electron temperature after sunset, resulting in a large downwards ion flux (*Farelo et al.*, 2002). In addition, during summer there is an upliftment of the F2-layer to regions of low recombination rates by equatorward meridonal winds (*Farelo et al.*, 2002). These effects result in a sharp increase in the number of ions and an enhancement is observed.

Daytime long duration Q-disturbances are thought to be related to variations of the atomic oxygen abundance in the thermosphere (*Mikhailov and Schlegel*, 2001). There exists a phenomenon known as the "forbidden time effect" for ionospheric storms where storms are seen less frequently in the midlatitude region during winter due to seasonal variations of the thermospheric wind (*Danilov*, 2013). The low frequency of occurrence of daytime Q-disturbances observed can be linked to this "forbidden time effect" (*Mikhailov et al.*, 2004). Negative daytime Q-disturbances result from a decrease in atomic

oxygen abundance, while positive daytime events near the equinoxes are related to the equinoctal transitions in atomic oxygen abundance (*Mikhailov et al.*, 2004). Significant differences have been noted between the seasonal behaviour over the African region and prior studies such as *Farelo et al.* (2002); *Mikhailov et al.* (2004). These differences are not yet understood and warrant further study.

4.5 Summary

In this chapter, the morphology of Q-disturbances over African latitudes has been explored. The observations were analysed in terms of time of occurrence, seasonal occurrence, duration and amplitude. The observed morphology is discussed and compared to suggested mechanisms from literature. Many features of Q-disturbance morphology in the equatorial region can be explained in terms of variations of $\mathbf{E}\times\mathbf{B}$. The morphology of Q-disturbances in the midlatitude region is not clearly explained in terms of any single mechanism. The mechanisms driving Q-disturbance formation in the midlatitudes will therefore be explored further in Chapter 5.

Chapter 5

Q-disturbances - Midlatitude Mechanisms

The morphology of Q-disturbances in the midlatitudes is complex and cannot be attributed to any single mechanism. Many mechanisms have been proposed for this region, as discussed in Section 4.4. Three proposed mechanisms have been selected for further analysis. These mechanisms are substorm activity, contribution of plasmaspheric TEC to GPS TEC and plasma transfer between conjugate points.

5.1 Substorm Activity and Q-disturbances

In order to explore the influence of substorm activity, the observed Q-disturbances were subdivided into Q-disturbances occurring under quiet or disturbed subauroral conditions. The AE index was considered to indicate elevated substorm activity when AE $>$ 200 nT (*Mikhailov and Perrone*, 2009). A Q-disturbance was considered to occur under disturbed subauroral conditions when the maximum AE-index during the Q-disturbance was AE $>$ 200 nT.

In Table 5.1, the percentage of all Q-disturbances occurring under disturbed auroral conditions, during solar minimum and solar maximum, is shown. Less than 7% of the total number of observed enhancements in 2013 and 11% of

depletions in 2009 are observed with AE > 200 nT. The results also show that more depletions than enhancements are associated with elevated substorm activity.

Table 5.1: Percentage of total number of median quiet time enhancements and percentage of total median number of quiet time depletions per station in the midlatitude region occurring with AE >200 nT with the median number of Q-disturbances occuring per station.

Type	Year	Total number of Q-disturbances	% of total
Enhancements	2009	22	5.8
	2013	19	6.9
Depletions	2009	28	10.9
	2013	19	11.0

Table 5.2 presents the percentage of Q-disturbances occurring under disturbed auroral conditions at solar minimum and maximum, respectively, commencing during different times of day. The percentages are calculated as the number of enhancements or depletions occurring under elevated substorm activity commencing in a single time sector divided by the total number of enhancements or depletions commencing in that time sector during the year in question. For example 15.8% of the total number of daytime enhancements during 2009 occurred under disturbed auroral conditions. The highest proportion of Q-disturbances occurring under disturbed auroral conditions are daytime disturbances, with 19% of daytime depletions during solar maximum occurring under elevated substorm activity and 18.2% of daytime depletions during solar maximum occurring under elevated substorm activity.

Nighttime enhancements occur under disturbed auroral conditions infrequently. A larger proportion of nighttime enhancements occur under disturbed subauroral conditions during solar maximum with 5.3% of pre-midnight enhancements and 3.8% of post-midnight enhancements occurring under elevated substorm activity. Nighttime depletions also occur less frequently under disturbed auroral conditions than daytime depletions, with 12.7% of pre-midnight

Table 5.2: The median total number of Q-disturbances per station and the corresponding percentage of Q-disturbances occurring under disturbed subauroral conditions in each time sector.

	Enhancement				Depletion			
	% 2009	Total 2009	% 2013	Total 2013	% 2009	Total 2009	% 2013	Total 2013
Daytime	15.8	7	18.2	4	18.0	3	19.0	4
Pre-midnight	0.0	3	5.3	6	2.8	5	12.7	5
Post-midnight	1.4	12	3.8	9	12.1	20	6.7	10

depletions occurring under elevated substorm activity during solar maximum and 12.1% of post-midnight depletions during solar minimum.

The low proportion of Q-disturbance events that can be related to an elevated AE index indicates that elevated substorm activity cannot be the sole or dominant mechanism driving the formation of Q-disturbances, as it leaves over 91% of Q-disturbances unexplained. Substorm activity also cannot be the only mechanism driving daytime Q-disturbances, as it does not play a role in over 82% of daytime Q-disturbances. It can be seen however, that a fractionally larger percentage of Q-disturbances occur under disturbed auroral conditions during solar maximum than during solar minimum. This is expected as there is a higher frequency of occurrence of geomagnetic disturbances during solar maximum than during solar minimum (*Davies*, 1989).

Figure 5.1 shows the probability distribution of the amplitude of Q-disturbances occurring under disturbed auroral conditions commencing at different times of day, given as a stacked fractional contribution to the overall probability of occurring in a specific amplitude band. The daytime enhancements occurring under elevated substorm activity at solar minimum most frequently have 45-55% amplitudes, which is also the most frequently observed amplitude seen for general quiet time enhancements in Figure 4.5. However, there is an equal probability of the daytime enhancement amplitude in the 55-85% bands during solar minimum as well as in the 65-85% and 95-105% bands during

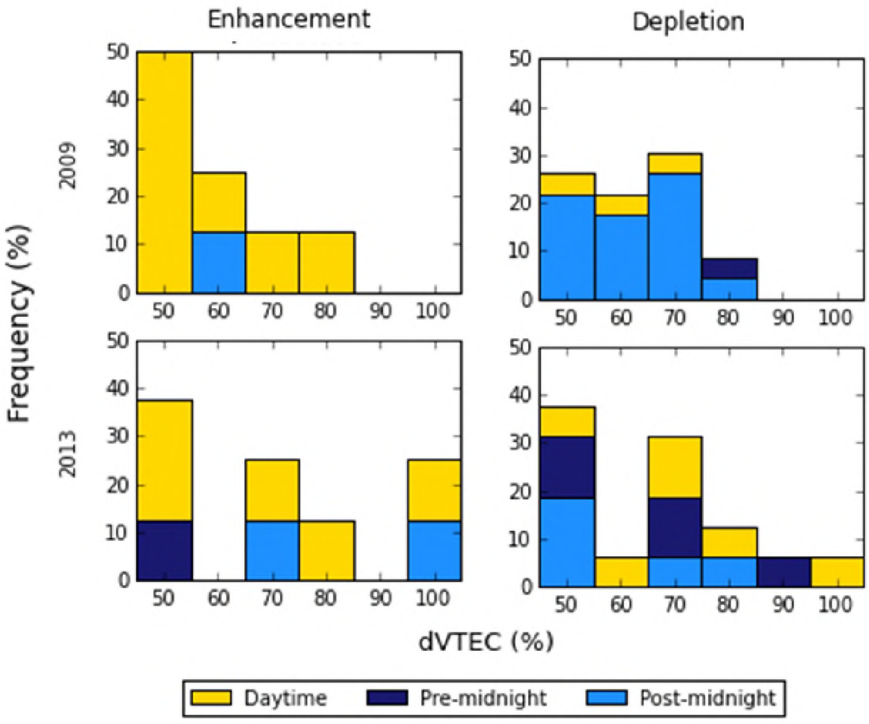

Figure 5.1: Amplitude (%dVTEC) of Q-disturbances occurring under disturbed subauroral conditions with daytime, pre- and post-midnight events are shown as a fractional contribution towards the overall occurrence probability.

solar maximum, which wasn't seen for general quiet time enhancements.

The post-midnight enhancements during solar minimum had amplitudes of 55-65%, while Figure 4.5 shows that the most frequent amplitude of general post-midnight solar minimum enhancements was 65-75%. However, during solar maximum, the post-midnight enhancements had amplitudes in the range of 65-75% and 95-105%, while the most common general amplitude for these enhancements is 45-55%, as show by Figure 4.5. The pre-midnight enhancements occurring during solar maximum under substorm conditions, have an amplitude of 45-55%, which matches the most frequently occurring amplitude of such enhancements. Enhancements occurring under elevated substorm activity had typical amplitudes (as illustrated in Figure 4.5), except for the post-midnight enhancements, which had smaller (larger) amplitudes during solar minimum (maximum) than the typical amplitudes.

No trend was observed for daytime depletions associated with disturbed auroral conditions during solar minimum, however these depletions mostly had amplitudes of 65-75% during solar maximum (see Figure 5.1). The pre-midnight depletions occurring during AE > 200 nT mostly had 45-55% and 65-75% amplitudes at solar maximum, while they had 75-85% amplitudes during solar minimum (as illustrated in Figure 5.1), which are larger than those occurring under general conditions (as shown in Figure 4.5).

Lastly Figure 5.1 illustrates that during solar maximum, the majority of post-midnight depletions occurring under disturbed substorm conditions had the same amplitudes as those under general conditions, but had larger amplitudes during solar minimum (65-75%); refer to Figure 4.5. The amplitude for depletions during solar minimum, illustrated in Figure 5.1, are larger than general quiet time depletions, as seen in Figure 4.5. This occurrence of larger depletions under disturbed auroral conditions is even more dominant during solar maximum.

Figure 5.2 shows the duration of Q-disturbances occurring under elevated substorm activity. Enhancements during solar minimum were of slightly longer duration (2.5-4.5 and 6.5-8.5 hours) than the typical duration (0.5-2.5 hours, as shown in Figure 4.4), as were the daytime and post-midnight enhancements during solar maximum. Pre-midnight enhancements during solar maximum were also longer (6.5-8.5 hours) than the corresponding general quiet time enhancements (0.5-4.5 hours as shown in Figure 4.4). Similar behaviour is seen for depletions occurring during disturbed auroral conditions.

The pre-midnight depletions during both solar minimum and solar maximum show typical durations (0.5-2.5 hours) but the duration of daytime depletions is longer (0.5-8.5 hours) than typical for those not occurring under disturbed auroral conditions (0.5-2.5 hours, as illustrated in Figure 4.4). This extended duration is particularly prominent for the post-midnight depletions

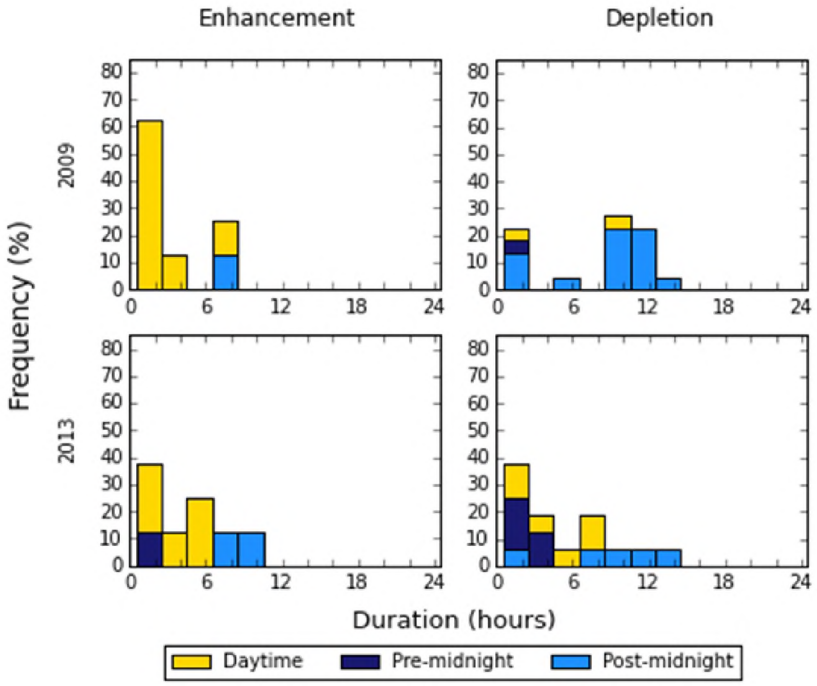

Figure 5.2: Duration of Q-disturbances occurring under disturbed subauroral conditions with daytime, pre- and post-midnight events are shown as a fractional contribution towards the overall occurrence probability.

during both solar minimum and solar maximum.

An increase in auroral activity causes heating in the auroral regions (*Mikhailov et al.*, 2012). This may result in equatorward travelling atmospheric disturbances, which cause a dampening of the solar driven thermospheric wind. This dampening of the thermospheric wind leads to downwelling of the neutral gas. Neutral gas downwelling causes an increase in the abundance of atomic oxygen in the subauroral and midlatitude regions. In addition, this results in a decrease of downwards plasma drift in the daytime region (*Mikhailov et al.*, 2012). This abundance of atomic oxygen, damped thermospheric wind and reduced plasma drift results in a slow return to equilibrium conditions, resulting in long duration enhancements. We would therefore expect that if the Q-disturbances observed under disturbed AE are affected by the auroral activity, these disturbances would be of longer duration than those occurring under undisturbed auroral conditions. This longer duration of quiet time enhancements is noted

in Figure 5.2.

5.2 The Role of the Plasmasphere

The plasmasphere can contribute to the occurrence of Q-disturbances through the transfer of plasma between conjugate points as well as through the contribution of the plasmasphere to GPS TEC measurements. *Lunt et al.* (1999a) found that for stations in the midlatitudes in the northern hemisphere, the plasmaspheric electron content of ray paths to the south of a GPS station are most significant, as could be expected from the known behaviour of the plasma and flux tube geometry. At solar minimum, this contribution in the European midlatitudes is small in absolute TECU but can constitute up to 50% of the TEC along a ray path at night during the winter months. The plasmaspheric contents were found to be approximately double in absolute magnitude during solar maximum but contribute a much smaller percentage of the TEC along the entire ray path.

In order to explore the role of the plasmaspheric contribution to GPS TEC, $dVTEC_{iono}$ was calculated according to Equation 3.45. This was completed using the procedure outlined in Section 3.2.2 for two midlatitude stations, namely HNUS and SPRT, as well as two conjugate stations, namely PENC and TUBI. These stations were chosen as they have the best matches for conjugate stations with data of an acceptable quality (a minimum of 65% data available).

The locations of these stations are illustrated by the red squares in Figure 3.5, and their coordinates are given in Table 5.3. As the plasmaspheric contribution to TEC is expected to be most significant during solar minimum (*Lunt et al.*, 1999a), the analysis was undertaken only for 2009.

Table 5.3: List of selected stations in the African midlatitude region with a corresponding geomagnetically conjugate station in the northern hemisphere. Geomagnetic coordinates listed were obtained from: http://www.ukssdc.ac.uk/cgi-bin/wdcc1/coordcnv.pl.

Hemisphere	Station ID	Geographic		Geomagnetic	
		latitude	longitude	latitude	longitude
South	SPRT	-24.67	30.19	-35.25	97.71
North	TUBI	40.78	29.45	35.06	101.91
South	HNUS	-34.43	19.22	-42.35	82.15
North	PENC	47.79	19.28	42.03	93.90

5.2.1 Ionospheric TEC

In this section, the occurrence of Q-disturbances in $dVTEC_{iono}$ will be explored and compared to the occurrence of Q-disturbances in $dVTEC_{GPS}$. As discussed in Section 3.2.1, a Q-disturbance was considered significant if $|dVTEC| > 45\%$. Once the plasmaspheric contribution has been removed, as per Equation 3.44, the amplitude of the dVTEC variations is altered and some events which were previously large enough to be significant, become non-significant. Table 5.4 shows the percentage of Q-disturbances that become non-significant after the plasmaspheric portion of $VTEC_{GPS}$ has been removed to calculate $dVTEC_{iono}$. Table 5.4 shows 23-65% of Q-disturbances become non-significant, indicating the plasmaspheric contribution during solar minimum is not negligible.

Table 5.4: Percentage of Q-disturbances which become non-significant after the plasmaspheric TEC has been removed.

Type	Day	Pre-midnight	Post-midnight
Enhancement	59.4	64.7	23.4
Depletion	50.0	57.1	54.5

The contribution of the plasmasphere to GPS TEC varies per disturbance. Table 5.5 presents the maximum and average plasmaspheric contribution, as a percentage, to the Q-disturbances that become non-significant once the plasmaspheric contribution is removed. The plasmaspheric contribution is

marginally larger in the post-midnight sector than the daytime and pre-midnight sectors. The results shown in Table 5.5 are in line with those presented in *Lunt et al.* (1999a). Specifically, *Lunt et al.* (1999a) noted that up to 50% of TEC during nighttime, at solar minimum, is attributable to the plasmasphere. Tables 5.4 and 5.5 show that the contribution of the plasmasphere to TEC is significant during Q-disturbances, however it does not fully account for the occurrence of Q-disturbances.

Table 5.5: Maximum and average percentage contribution of plasmaspheric TEC to Q-disturbances.

Type	Plasma contribution	Day	Pre-midnight	Post-midnight
Enhancement	Maximum	32.7	32.3	42.8
	Average	18.8	20.5	24.7
Depletion	Maximum	38.2	19.3	39.3
	Average	26.0	11.9	20.3

Zhang et al. (2017) noted that there is a strong annual variation of plasmaspheric TEC with the lowest plasmaspheric TEC observed during the June solstice and the highest plasmaspheric TEC observed during the December solstice, in the longitudes 240°E to 60°E. In addition, *Zhang et al.* (2017) noted very weak seasonal variations of the plasmaspheric TEC in the longitudes 60°E to 240°E.

The majority of studies use ionosonde data to determine Q-disturbance morphology, while those using GPS TEC were mostly in the 60° to 240° region. These previous studies noted a seasonal variation, with more Q-disturbances occurring during winter. This seasonal variation was notably absent in our GPS TEC observations over Africa. This lack of seasonal variation in our Q-disturbance observations may be attributable to the plasmaspheric contribution to GPS TEC measurements, and the seasonal variation thereof.

5.2.2 Plasmaspheric Transfer between Conjugate Points

Geomagnetically conjugate points on the Earth's surface experience transfer of plasma between the ionosphere above these regions. This is due to the plasmasphere forming a mutual reservoir that links the ionosphere between the northern and southern hemispheres.

Farelo et al. (2002) suggested this transfer of plasma could be a mechanism driving Q-disturbances, as discussed in Section 4.4. In order to explore the transfer of plasma between conjugate points as a possible driver of Q-disturbances, $dVTEC_{GPS}$ presented in Section 5.2.1 for HNUS and SPRT were compared to those calculated for PENC and TUBI.

Figure 5.3 shows the number of Q-disturbances for PENC, TUBI, HNUS and SPRT commencing in the daytime, pre- and post-midnight sectors. Figure 5.4 shows the percentage of Q-disturbances occurring in each season for the northern and southern hemispheres.

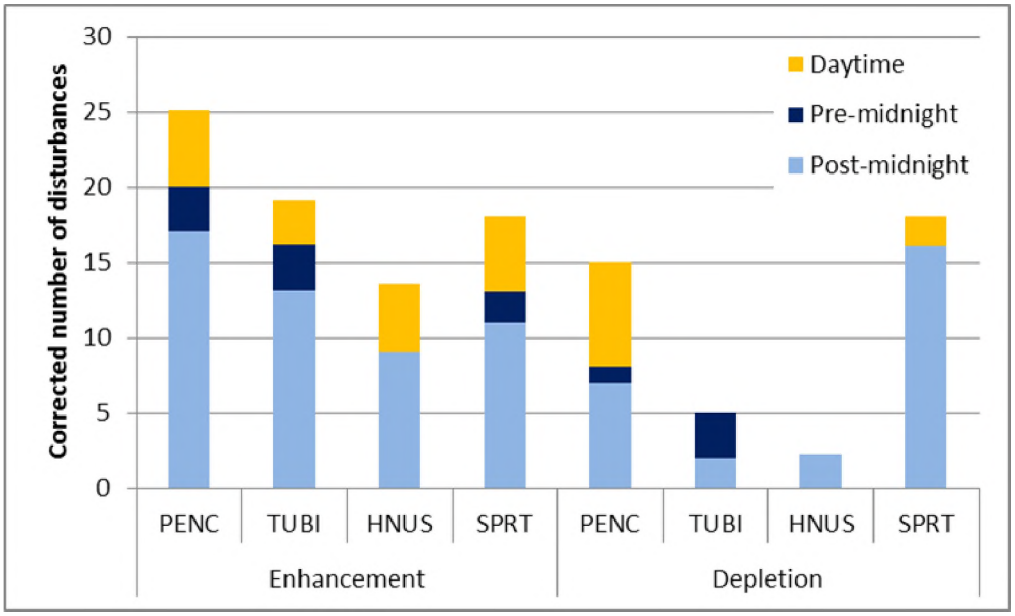

Figure 5.3: Number of Q-disturbances at PENC, TUBI, HNUS and SPRT for 2009.

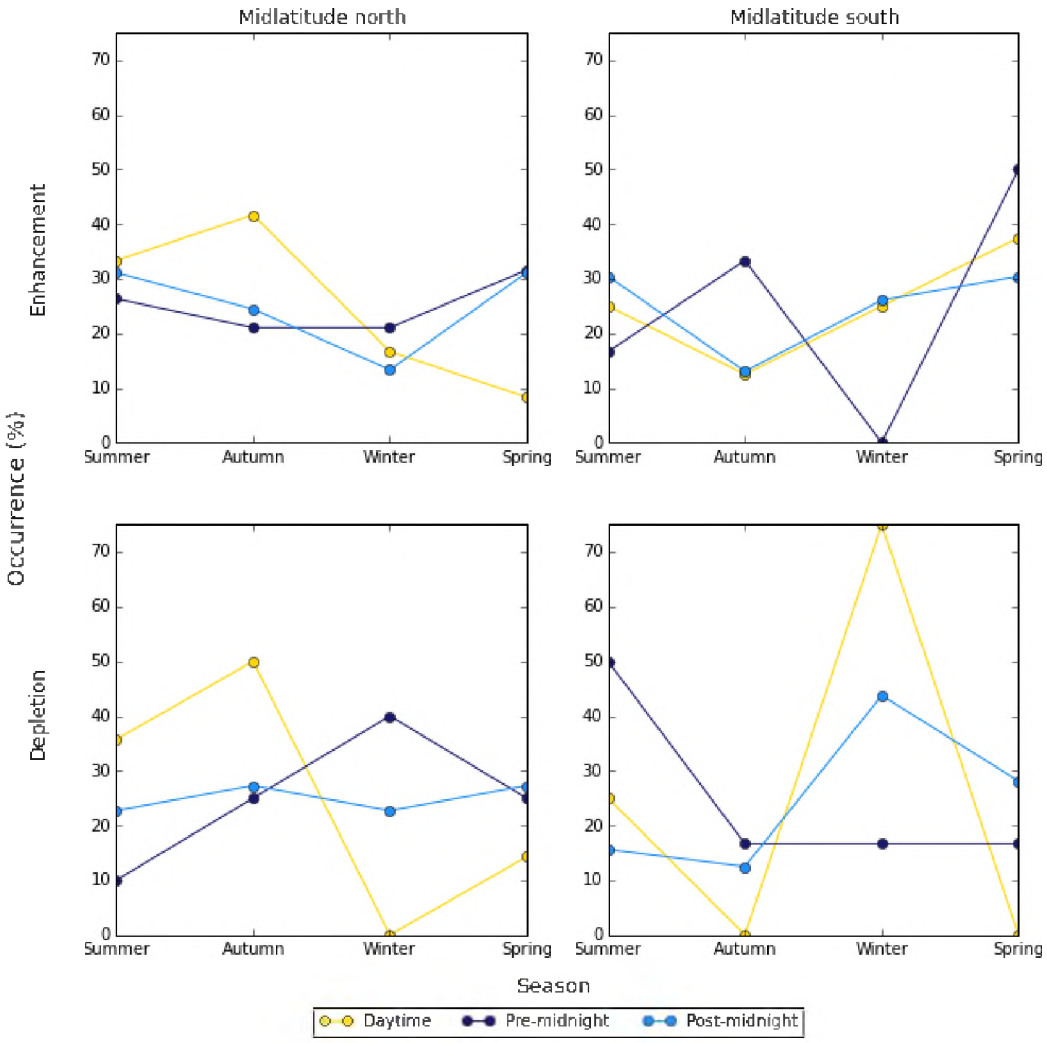

Figure 5.4: Number of Q-disturbances at conjugate stations per region as a percentage occurrence per season.

The seasons in Figure 5.4 are taken to be summer (winter) from December to February, autumn (spring) from March to May, winter (summer) from June to August and spring (autumn) from September to November in the southern (northern) hemisphere. If conjugate plasma transfer is driving the occurrence of Q-disturbances, one would expect a transfer of plasma in the direction of the prevailing background thermospheric circulation.

The prevailing winds are equatorward except for winter at night when the circulation is poleward (*Danilov*, 2013) as illustrated in Figure 5.5. This means that a transfer of plasma from the summer nighttime side of the Earth to the winter nighttime side of the Earth would result. In all other scenarios, the wind from both the northern and southern hemisphere blow towards the equator and no transfer is expected between conjugate stations. Thus, where one station sees a high number of depletions during the nighttime in summer, we would expect the conjugate station to see a high number of enhancements (in the nighttime winter region).

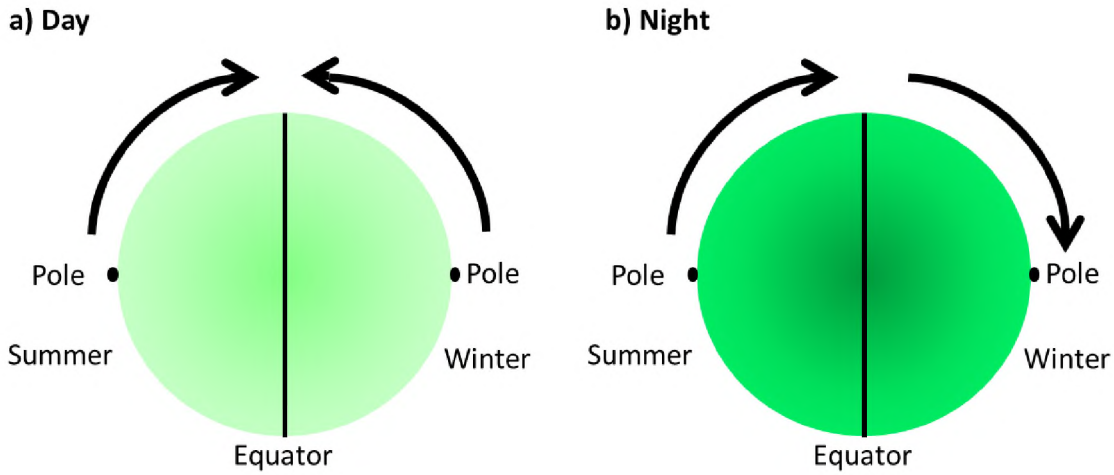

Figure 5.5: Direction of background thermospheric wind in the summer and winter hemispheres for a) daytime and b) nighttime.

Figure 5.6 shows the day-night enhancement-depletion occurrence at the conjugate station pairs, TUBI-SPRT and PENC-HNUS. If plasma transfer between conjugate stations is a strong mechanism, we would expect to see a correspondence between the number of nighttime summer depletions and nighttime winter enhancements in opposite hemispheres. This does not appear to be the case for either of the conjugate pairs under consideration. As illustrated in Figure 5.4, this also does not appear to be the case when averaging the stations in the separate hemispheres. This suggests that conjugate transfer is not a dominant mechanism in the formation of Q-disturbances.

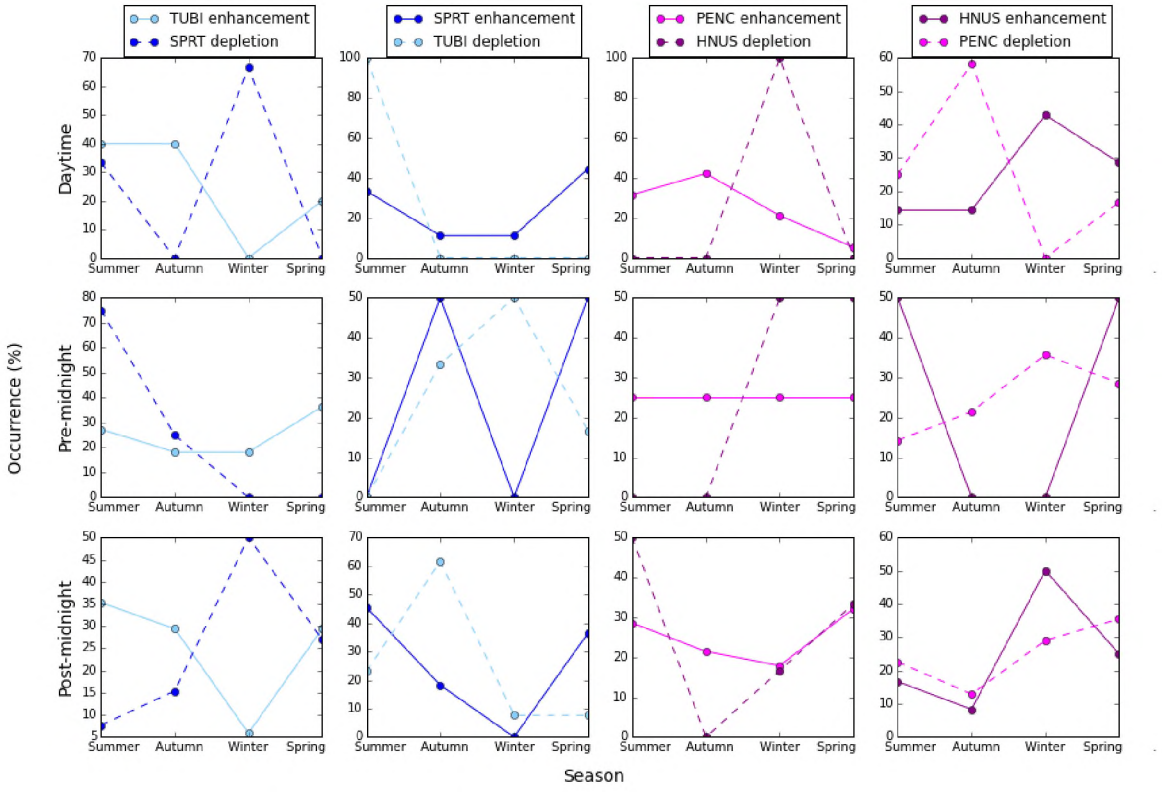

Figure 5.6: Number of Q-disturbances at each station as a percentage occurrence per season, paired as enhancements and depletions at conjugate stations in opposite hemispheres.

5.3 Summary

In this chapter, substorm activity, plasma transfer between conjugate points and the effects of the plasmasphere on GPS TEC measurements were explored in more depth as potential mechanisms driving Q-disturbances in the midlatitude region. Although some Q-disturbances occur during substorm activity, this mechanism still leaves the majority of Q-disturbances observed in this study unexplained. This indicates that substorm activity is neither the sole nor the dominant mechanism in the formation of Q-disturbances. The morphology of Q-disturbances occurring under disturbed auroral conditions differs somewhat from general Q-disturbance morphology, with Q-disturbances occurring under elevated substorm conditions having a higher probability of being longer and having a larger amplitude than general Q-disturbances. This suggests that substorm activity could either be a minor contributing mechanism or that elevated substorm conditions that occur simultaneously with a Q-disturbance affect the character of that disturbance.

The effects of the plasmasphere on GPS TEC are significant and contribute to over half of all daytime and pre-midnight Q-disturbances during solar minimum, as well as more than 25% of post-midnight Q-disturbances. This suggests that GPS TEC measurements of the ionosphere need to take into account the influence of the plasmasphere during quiet times.

The transfer of plasma between conjugate ionospheric stations does not appear to be a significant mechanism in the formation of the observed Q-disturbances over the African region. The expected correspondence between enhancements and depletions in opposite hemispheres was not identified when comparing either the conjugate pairs individually or the average station results. This suggests that the transfer of plasma between conjugate stations does not significantly affect the character of the Q-disturbances.

Chapter 6

Pre-storm and Quiet Time Enhancements

One of the primary questions of this thesis is whether pre-storm enhancements are quiet time ionospheric enhancements that coincidentally occur prior to geomagnetic disturbances or are a separate phenomenon. In order to address this, all the quiet time enhancements that meet the criteria for being a pre-storm enhancement are identified.

The pre-storm enhancements are the subset of quiet time enhancements that occur within 24 hours prior to a geomagnetic disturbance. The characteristics of these pre-storm enhancements have been compared to the characteristics of the quiet time enhancements and the implications of this are discussed.

Table 6.1 presents the quiet time enhancements starting within 24 hours prior to a Dst disturbance showing the geomagnetic disturbance commencement time (day of year), minimum associated Dst (nT) with the region where the pre-storm enhancement was observed, the time of day of pre-storm enhancement commencement and the duration and amplitude (% dVTEC) for each pre-storm enhancement.

Table 6.1: Geomagnetic storms and corresponding pre-storm enhancements and their properties.

Storm Start	Min Dst (nT)	Region	Time	Duration	dVTEC (%)
203 (2009)	-83.0	Equatorial crest	Pre	1h13m	63
76 (2013)	-132.0	Midlatitude	Pre	0h48m - 1h52m	50 - 68
195 (2013)	-36.0	Midlatitude	Day	0h43m	51
287 (2013)	-37.0	Midlatitude	Post	0h56m	55
313 (2013)	-81.0	Equatorial crest	Pre	0h48m	46

The year 2009 was a geomagnetically quiet year, where only 6 events with Dst < -30 nT were observed. Of the 200 quiet time enhancements observed over Africa during 2009, only one occurred within 24 hours prior to a geomagnetic disturbance. The year 2013 was a more geomagnetically disturbed period, with 66 events observed to have Dst < -30 nT, but of the 230 enhancements observed, only 4 were associated with pre-storm events.

This means that during 2009, only 17% of geomagnetic disturbances had an accompanying pre-storm enhancement. During 2013, only 6% of geomagnetic disturbances had an accompanying pre-storm enhancement. This decreased frequency of occurrence during solar maximum agrees with the observations in *Burešová and Laštovička* (2007, 2008), who noted that pre-storm enhancements were seldom observed or even absent during solar maximum. The observed frequency of occurrence of pre-storm enhancements during solar minimum in this study is however much lower than the results of *Burešová and Laštovička* (2007), who found 15-20% of geomagnetic disturbances were accompanied by pre-storm enhancements. *Burešová and Laštovička* (2007) used foF2 data, as opposed to TEC data used in this study, and they have different lower limits of significant disturbances to this work, which will account for differences in the qualitative results.

In order to determine whether pre-storm enhancements are a special case of quiet time enhancements, the characteristics of the observed pre-storm enhancements will be compared with the morphology of quiet time enhancements

presented in Chapter 4. The single pre-storm enhancement observed during 2009 was observed at MBAR in the equatorial crest region. It was observed during the pre-midnight period, which is the most likely time for a quiet time enhancement to be observed during solar minimum in this region. This pre-storm enhancement had a duration of 1h13m and an amplitude of 63%, which is also the most frequently observed duration and amplitude for pre-midnight quiet time enhancements during solar minimum in the equatorial crest region, as shown in Chapter 4.

Four pre-storm enhancements were observed during 2013, of which one was observed simultaneously at three midlatitude stations. The pre-storm enhancement observed at multiple stations was seen at DRBN, SBOK and WIND on day 76 of 2013, and showed a decreasing duration moving equatorward. The amplitude of this pre-storm enhancement was also largest at the southernmost station, DRBN. This event was observed in the pre-midnight hours, which is the least likely time for quiet time enhancements in the midlatitude region during solar minimum. The duration of this enhancement was 0h48m-1h52m over the three stations. The most frequently observed duration for pre-midnight enhancements in the midlatitude region during solar minimum is 0h30m-2h00m. The observed amplitudes at WIND and SBOK of 50% and 52%, respectively, fall within the most frequently observed amplitude band of 45-65%, for this region. The amplitude of 68% observed at DRBN is slightly higher than the average enhancement for this region, but smaller than the largest observed amplitudes, as illustrated in Figure 4.4.

An additional two of the four pre-storm enhancements observed during 2013 were observed in the midlatitude region. The first of these two pre-storm enhancements was a daytime enhancement observed at HNUS, while the second pre-storm enhancements was a post-midnight enhancement observed at SBOK. The observed duration (43 min, 56 min) and amplitude (51, 55%) match those most frequently seen for such enhancements.

The fourth pre-storm enhancement seen in 2013 was observed in the equatorial region at MBAR and is associated with a geomagnetic disturbance of a similar strength to the one observed in 2009 commencing during the same time of day, i.e. in the pre-midnight sector. However, this pre-storm enhancement was smaller and of shorter duration than the one observed during 2009. The duration of this pre-storm (48 min) lies within the most frequently observed duration (30 min - 2h30min)for pre-midnight equatorial crest enhancements during 2013, while the amplitude of the pre-storm (46%) is commonly seen, but not the most frequently seen amplitude (55-65%).

The characteristics of the observed pre-storm enhancements generally fall within the most frequently observed duration and amplitude of quiet time enhancements. Similar to the observations in *Burešová and Laštovička* (2007), the pre-storm enhancements are observed during both the day and nighttime. Although the sample size is too small to be definitive, the characteristics of pre-storm quiet time enhancements and general quiet time enhancements do not seem differentiable. This means that if pre-storm enhancements are a real phenomenon, they would be a poor predictor for geomagnetic disturbances as they are rarely observed and are not distinctly different from quiet time enhancements.

6.1 Summary

In this chapter the properties of quiet time enhancements which occur within 24 hours prior geomagnetic storm were explored. These properties were then compared to those of general quiet time enhancements. The observations suggest that pre-storm enhancements would be a poor prediction mechanism for geomagnetic disturbances as they are not clearly differentiable from quiet time enhancements not occurring within 24 hours of a geomagnetic disturbance, which are much more numerous as well.

Chapter 7

Summary and Future Work

In this thesis, a characterisation of the morphology of Q-disturbances was undertaken over African latitudes under solar minimum and maximum conditions. The observed behaviour was analysed to gain insight into the mechanisms driving the formation of Q-disturbances. A more in depth analysis of the mechanisms driving Q-disturbances in the midlatitude region was undertaken. An analysis of the frequency of occurrence of pre-storm enhancements together with their characteristics was undertaken to gain insight into the potential of pre-storm enhancements as a predictor of geomagnetic disturbances as well as to gain insight as to whether pre-storm enhancements are a special case of quiet time enhancements.

7.1 Q-disturbance Morphology

This study explored Q-disturbances over different latitude sectors over the African region during both solar minimum (2009) and solar maximum (2013). The results of this study show that while many of the observed morphological features are similar to those observed over other regions, there are notable differences, some of which may be attributable to the contributions of a standing planetary wave. The observations over the equatorial region show that variations of the $\mathbf{E}\times\mathbf{B}$ drift are able to explain the majority of the observed morphological features, strengthening assertions by *Depueva et al.* (2005) and

Depuev et al. (2008) that the **E**×**B** drift is the dominant mechanism in the equatorial region.

Conversely, the morphological features of the midlatitude region are not attributable to a single mechanism, with several different mechanisms contributing to the overall observed behaviour. Some notable morphological features of this study are as follows:

- nighttime Q-disturbances are seen more frequently than daytime disturbances,
- negative Q-disturbances occur most frequently in the post-midnight sector,
- in the equatorial regions, more Q-disturbances are seen at solar maximum. However, in the midlatitude region more Q-disturbances are seen at solar minimum,
- no pronounced seasonal trend in occurrence is seen over the African sector,
- the majority of Q-disturbances have a duration ≤ 3 hours. The longest and largest Q-disturbances occur during solar minimum with frequency of long duration and large amplitude events increasing towards higher latitudes,
- Q-disturbances in the equatorial ionosphere are caused by variations in the **E**×**B** drift and the geophysical variations thereof, and
- a number of mechanisms influence Q-disturbances at midlatitudes, including substorm activity, plasmaspheric influx, thermospheric winds and neutral composition.

This study has given us further insight into the mechanisms driving the formation of Q-disturbances. In particular, it lends support to the suggestions of previous studies in the American and Asian regions that Q-disturbances in

the equatorial region are largely driven by variations in the $\mathbf{E}\times\mathbf{B}$ drift. The lack of a dominant seasonal behaviour in the Q-disturbances observed over the African equatorial region in this study could fit into the seasonal standing planetary wave postulate proposed by *Depueva et al.* (2005) and this requires further investigation.

7.2 Mechanisms in the Midlatitude Region

The relationship between substorm activity and the occurrence of Q-disturbances was investigated. Substorm activity was not found to be a major contributor to the formation of Q-disturbances, however the morphology of Q-disturbances occurring under elevated substorm conditions differed from that of general Q-disturbances, suggesting there is a relationship between Q-disturbances and elevated substorm conditions.

The role of the plasmasphere in GPS TEC measurements was analysed by determining the ionospheric TEC using the Constellation Observing System for Metrology, Ionosphere and Climate (COSMIC) satellite array, with six satellites in 72° inclination orbits at an altitude of ~800 km. More information on COSMIC can be found in *Pedatella and Larson* (2010) and *Yue et al.* (2011). The effect of the plasmasphere was found to be significant, with a substantial number of Q-disturbances becoming insignificant once the plasmaspheric contribution to GPS TEC was removed. The role of plasma transfer between conjugate points was also analysed, using two midlatitude conjugate pairs. If conjugate transfer was a dominant mechanism, a correlation between nighttime depletions in the summer hemisphere and nighttime enhancements in the winter hemisphere would be expected. This correlation is not observed in the selected conjugate pairs, suggesting that conjugate transfer is not a mechanism driving Q-disturbance formation.

7.3 Pre-storm Enhancements

The frequency of occurrence of quiet time enhancements prior to geomagnetic disturbances was analysed for solar minimum and solar maximum. Pre-storm enhancements were infrequently observed, suggesting that they are a poor predictor of geomagnetic disturbances. In addition, the characteristics of pre-storm enhancements were contrasted against those of general quiet time enhancements. There was a large similarity in the characteristics of pre-storm and quiet time enhancements, suggesting pre-storm enhancements are unlikely to be a separate sub-class of quiet time enhancements with distinct characteristics.

7.4 Future Work

This work is limited by the spatial and temporal availability of data over the African region, as well as the low quality of some of the available data. A more complete morphology of Q-disturbances over the African region would ideally include data for multiple solar cycles, in order to give a more statistical analysis of the occurrence and behaviour of Q-disturbances at solar minimum and solar maximum. In addition, the morphology across a full solar cycle could give more insight as to the influence of solar activity on the occurrence and characteristics of Q-disturbances. Extension over a full solar cycle or multiple solar cycles would also allow for more pre-storm events to be included in the analysis. This would allow a more complete comparison of pre-storm enhancement characteristics with quiet time enhancement morphology, thus giving a stronger indication of whether pre-storm enhancements are a special case of quiet time enhancements.

A larger number of stations, particularly in the equatorial regions would also allow the formation of a more statistically complete morphology for Q-disturbances in the region. Currently there are not enough equatorial stations with suitable data quality. In addition, as the phenomenon of equatorial

spread F causes ionospheric depletions in the $\pm 20°$ latitude region, the contribution of this phenomenon to equatorial depletions should be considered (*Paznukhov et al.*, 2012). This phenomenon would most likely have a contribution during the post sunset hours, particularly during the equinoxes. The link between $\mathbf{E} \times \mathbf{B}$ variations and the occurence of Q-disturbances in the equatorial region could be further strengthened by using $\mathbf{E} \times \mathbf{B}$ observations obtained from satellites such as Communications/Navigation Outage Forecasting System (C/NOFs) and Defense Meteorological Satellite Program (DMSP).

An extension of the region of study to include the northern hemisphere, particularly including more conjugate station pairs would help build a more decisive understanding of the role of conjugate transfer of plasma between the hemispheres and it's role in the formation of Q-disturbances. Inclusion of the northern hemisphere would also allow for comparison between GPS TEC and ionospheric TEC, as this is not possible over the African region due to the low number of ionosondes and data gaps during which limited ionosonde data is available. Including an analysis of the contribution of the plasmasphere to GPS TEC during solar maximum would also give a more complete understanding of the influence of the plasmasphere on Q-disturbance occurrence as well as the role of plasmaspheric transfer between conjugate points. The role of long-period gravity waves as a potential source of Q-disturbances may also be investigated, although this mechanism is expected to result in a small contribution due to the high amplitude limit used as a lower limit of significant Q-disturbances in this study.

Over the African midlatitude region, a distinct lack of seasonal trend was observed, which differs from the winter dominance of depletions shown by *Farelo et al.* (2002) and *Mikhailov et al.* (2004). This difference may be attributable to the use of GPS TEC and the seasonal character of the plasmaspheric contribution to these readings and warrants further investigation. Also, using the quiet time morphology obtained, it can be investigated whether there

is a distinction between earthquake-induced ionospheric F2-layer disturbances and Q-disturbances, as discussed in *Xu et al.* (2015), although the disturbances proposed to be linked to earthquakes may be too small to be included as Q-disturbances by the criteria of this study.

Chapter 8

References

Adekoya, B. J., V. U. Chukwuma, N. O. Bakare, and T. W. David, On the effects of geomagnetic storms and pre storm phenomena on low and middle latitude ionospheric F2, *Astrophysics & Space Science*, *340*, 217–235, doi: 10.1007/s10509-012-1082-x, 2012.

Bailey, G. J., R. J. Moffett, and J. A. Murphy, Interhemispheric flow of thermal plasma in a closed magnetic flux tube at mid-latitudes under sunspot minimum conditions, *Planetary and Space Science*, *26*, 753–765, doi:10.1016/0032-0633(78)90006-5, 1978.

Balan, N., Y. Otsuka, T. Tsugawa, S. Miyazaki, T. Ogawa, and K. Shiokawa, Plasmaspheric electron content in the GPS ray paths over Japan under magnetically quiet conditions at high solar activity, *Earth, Planets, and Space*, *54*, 71–79, 2002.

Bartels, J., and J. Veldkamp, International Data on Magnetic Disturbances, First Quarter, 1949, *Journal of Geophysical Research*, *54*, 295–299, doi: 10.1029/JZ054i003p00295, 1949.

Blagoveshchensky, D. V., and A. S. Kalishin, Increase in the critical frequency of the ionospheric F region prior to the substorm expansion phase, *Geomagnetism and Aeronomy*, *49*, 200–209, doi:10.1134/S0016793209020091, 2009.

Blagoveshchensky, D. V., J. W. MacDougall, and A. V. Piatkova, Ionospheric effects preceding the October 2003 Halloween storm, *Journal of Atmospheric and Solar-Terrestrial Physics*, *68*, 821–831, doi:10.1016/j.jastp.2005.10.017, 2006.

Buonsanto, M. J., Ionospheric Storms - A Review, *Space Science Reviews*, *88*, 563–601, doi:10.1023/A:1005107532631, 1999.

Burešová, D., and J. Laštovička, Pre-storm enhancements of foF2 above Europe, *Advances in Space Research*, *39*, 1298–1303, doi:10.1016/j.asr.2007.03.003, 2007.

Burešová, D., and J. Laštovička, Pre-storm electron density enhancements at middle latitudes, *Journal of Atmospheric and Solar-Terrestrial Physics*, *70*, 1848–1855, doi:10.1016/j.jastp.2008.01.014, 2008.

Carpenter, D. L., and C. G. Park, On what ionospheric workers should know about the plasmapause-plasmasphere., *Reviews of Geophysics and Space Physics*, *11*, 133–154, doi:10.1029/RG011i001p00133, 1973.

Chappell, C. R., Recent satellite measurements of the morphology and dynamics of the plasmasphere., *Reviews of Geophysics and Space Physics*, *10*, 951–979, doi:10.1029/RG010i004p00951, 1972.

Chukwuma, V. U., On ionospheric phenomena during pre-storm and main phase of a very intense geomagnetic storm, *Acta Geophysica*, *58*, 1164–1192, doi:10.2478/s11600-010-0008-7, 2010.

Danilov, A. D., F2-region response to geomagnetic disturbances, *Journal of Atmospheric and Solar-Terrestrial Physics*, *63*, 441–449, doi:10.1016/S1364-6826(00)00175-9, 2001.

Danilov, A. D., Ionospheric F-region response to geomagnetic disturbances, *Advances in Space Research*, *52*, 343–366, doi:10.1016/j.asr.2013.04.019, 2013.

Danilov, A. D., and D. D. Belik, Thermosphere-ionosphere interaction in a period of ionosphere storms., *Geomagnetism and Aeronomy*, *31*, 157–167, 1991.

Davies, K., *Ionospheric radio*, 31, Peter Perigrinus, 1989.

Davis, T. N., and M. Sugiura, Auroral electrojet activity index AE and its universal time variations, *Journal of Geophysical Research*, *71*, 785–801, doi:10.1029/JZ071i003p00785, 1966.

Depuev, V., A. Depueva, and T. Y. Leshchinskaya, Mechanism of formation of Q-disturbances in the F2 region of the equatorial ionosphere, *Geomagnetism and Aeronomy*, *48*, 89–97, doi:10.1007/s11478-008-1010-y, 2008.

Depueva, A. K., A. V. Mikhailov, and V. K. Depuev, Quiet time F2-layer disturbances at geomagnetic equator, *International Journal of Geomagnetism and Aeronomy*, *5*, GI3001, doi:10.1029/2004GI000071, 2005.

Farelo, A. F., M. Herraiz, and A. V. Mikhailov, Global morphology of night-time NmF2 enhancements, *Annales Geophysicae*, *20*, 1795–1806, doi: 10.5194/angeo-20-1795-2002, 2002.

Fejer, B. G., S. A. Gonzalez, E. R. de Paula, and R. F. Woodman, Average vertical and zonal F region plasma drifts over Jicamarca, *Journal of Geophysical Research*, *96*, 13, doi:10.1029/91JA01171, 1991.

Fisher, G., and J. Kunches, Building resilience of the Global Positioning System to space weather, *Space Weather*, *9*, S12004, doi: 10.1029/2011SW000718, 2011.

Foelsche, U., and G. Kirchengast, A simple "geometric" mapping function for the hydrostatic delay at radio frequencies and assessment of its performance, *Geophysical Research Letters*, *29*, 1473, doi:10.1029/2001GL013744, 2002.

Gonzalez, W. D., J. A. Joselyn, Y. Kamide, H. W. Kroehl, G. Rostoker, B. T. Tsurutani, and V. M. Vasyliunas, What is a geomagnetic storm?, *Journal of Geophysical Research*, *99*, 5771–5792, doi:10.1029/93JA02867, 1994.

Hargreaves, J., *The Solar-Terrestrial Environment: An Introduction to Geospace - the Science of the Terrestrial Upper Atmosphere, Ionosphere, and Magnetosphere*, Cambridge Atmospheric and Space Science Series, Cambridge University Press, 1992.

Hedin, A. E., MSIS-86 thermospheric model, *Journal of Geophysical Research*, *92*, 4649–4662, doi:10.1029/JA092iA05p04649, 1987.

Hernández-Pajares, M., A. GarcíA-Rigo, J. M. Juan, J. Sanz, E. Monte, and A. Aragón-ÀNgel, GNSS measurement of EUV photons flux rate during strong and mid solar flares, *Space Weather*, *10*, S12001, doi: 10.1029/2012SW000826, 2012a.

Hernández-Pajares, M., J. M. Juan, J. Sanz, and A. Aragón-Àngel, Propagation of medium scale traveling ionospheric disturbances at different latitudes and solar cycle conditions, *Radio Science*, *47*, RS0K05, doi: 10.1029/2011RS004951, 2012b.

Hofmann-Wellenhof, B., H. Lichtenegger, and J. Collins, *Global Positioning System: theory and practice*, Springer-Verlag, 1997.

Kane, R. P., Global evolution of F2-region storms, *Journal of Atmospheric and Terrestrial Physics*, *35*, 1953, 1973.

Kane, R. P., Ionospheric foF2 anomalies during some intense geomagnetic storms, *Annales Geophysicae*, *23*, 2487–2499, doi:10.5194/angeo-23-2487-2005, 2005.

Liu, L., W. Wan, M.-L. Zhang, and B. Zhao, Case study on total electron content enhancements at low latitudes during low geomagnetic activities before the storms, *Annales Geophysicae*, *26*, 893–903, doi:10.5194/angeo-26-893-2008, 2008a.

Liu, L., W. Wan, M.-L. Zhang, B. Zhao, and B. Ning, Prestorm enhancements in NmF_2 and total electron content at low latitudes, *Journal of Geophysical Research (Space Physics)*, *113*, A02311, doi:10.1029/2007JA012832, 2008b.

Liu, L., B. Zhao, W. Wan, B. Ning, M.-L. Zhang, and M. He, Seasonal variations of the ionospheric electron densities retrieved from Constellation Observing System for Meteorology, Ionosphere, and Climate mission radio occultation measurements, *Journal of Geophysical Research (Space Physics)*, *114*, A02302, doi:10.1029/2008JA013819, 2009.

Lunt, N., L. Kersley, and G. J. Bailey, The influence of the protonosphere on GPS observations: Model simulations, *Radio Science*, *34*, 725–732, doi:10.1029/1999RS900002, 1999a.

Lunt, N., L. Kersley, G. J. Bishop, A. J. Mazzella, and G. J. Bailey, The effect of the protonosphere on the estimation of GPS total electron content: Validation using model simulations, *Radio Science*, *34*, 1261–1271, doi:10.1029/1999RS900043, 1999b.

Mannucci, A. J., B. A. Iijima, J. J. Lindqwister, L. Sparks, and B. D. Wilson, GPS and Ionosphere, *The Review of Radio Science*, 1996.

Mansilla, G. A., Ionospheric effetcs of an intense geomagnetic storm, *Studia Geophysica et Geodaetica*, *51*, 563–574, doi:10.1007/s11200-007-0033-4, 2007.

Matamba, T. M., J. B. Habarulema, and L.-A. McKinnell, Statistical analysis of the ionospheric response during geomagnetic storm conditions over south africa using ionosonde and gps data, *Space Weather*, *13*(9), 536–547, 2015.

Mazzella, A. J., Plasmasphere effects for GPS TEC measurements in North America, *Radio Science*, *44*, RS5014, doi:10.1029/2009RS004186, 2009.

McNamara, L., *The Ionosphere: Communications, Surveillance, and Direction Finding*, Orbit, a foundation series, Krieger Publishing Company, 1991.

Mendillo, M., Storms in the ionosphere: Patterns and processes for total electron content, *Reviews of Geophysics*, *44*, RG4001, doi:10.1029/2005RG000193, 2006.

Mikhailov, A. V., and L. Perrone, Pre-storm NmF2 enhancements at middle latitudes: delusion or reality?, *Annales Geophysicae*, *27*, 1321–1330, doi: 10.5194/angeo-27-1321-2009, 2009.

Mikhailov, A. V., and K. Schlegel, Equinoctial transitions in the ionosphere and thermosphere, *Annales Geophysicae*, *19*, 783–796, doi:10.5194/angeo-19-783-2001, 2001.

Mikhailov, A. V., A. K. Depueva, and T. Y. Leschinskaya, Morphology of quiet time F2-layer disturbances: High to lower latitudes, *International Journal of Geomagnetism and Aeronomy*, *5*, GI1006, doi:10.1029/2003GI000058, 2004.

Mikhailov, A. V., A. H. Depueva, and V. H. Depuev, Daytime F2-layer negative storm effect: what is the difference between storm-induced and Q-disturbance events?, *Annales Geophysicae*, *25*, 1531–1541, doi: 10.5194/angeo-25-1531-2007, 2007.

Mikhailov, A. V., A. H. Depueva, and V. H. Depuev, Quiet time F2-layer disturbances: seasonal variations of the occurrence in the daytime sector, *Annales Geophysicae*, *27*, 329–337, doi:10.5194/angeo-27-329-2009, 2009.

Mikhailov, A. V., L. Perrone, and N. V. Smirnova, Two types of positive disturbances in the daytime mid-latitude F2-layer: Morphology and formation mechanisms, *Journal of Atmospheric and Solar-Terrestrial Physics*, *81*, 59–75, doi:10.1016/j.jastp.2012.04.003, 2012.

Parkinson, B., and J. Spilker, *Global Positioning System: Theory and Applications*, no. v. 1 in Ciencia militar y naval, American Institute of Aeronautics & Astronautics, 1996.

Paznukhov, V. V., et al., Equatorial plasma bubbles and L-band scintillations in Africa during solar minimum, *Annales Geophysicae*, *30*, 675–682, doi: 10.5194/angeo-30-675-2012, 2012.

Pedatella, N. M., and K. M. Larson, Routine determination of the plasmapause based on COSMIC GPS total electron content observations of the

midlatitude trough, *Journal of Geophysical Research (Space Physics)*, *115*, A09301, doi:10.1029/2010JA015265, 2010.

Rishbeth, H., and O. K. Garriott, *Introduction to ionospheric physics*, 1969.

Sardon, E., A. Rius, and N. Zarraoa, Estimation of the transmitter and receiver differential biases and the ionospheric total electron content from Global Positioning System observations, *Radio Science*, *29*, 577–586, doi:10.1029/94RS00449, 1994.

Schrijver, C. J., et al., Understanding space weather to shield society: A global road map for 2015-2025 commissioned by COSPAR and ILWS, *Advances in Space Research*, *55*, 2745–2807, doi:10.1016/j.asr.2015.03.023, 2015.

Seemala, G. K., and C. E. Valladares, Statistics of total electron content depletions observed over the South American continent for the year 2008, *Radio Science*, *46*, RS5019, doi:10.1029/2011RS004722, 2011.

Sugiura, M., and T. Kamei, Equatorial Dst index 1957–1986, IAGA Bull., 40, ISGI Pub, *Office, Saint-Maur-des-Fossess, France*, 1991.

Xu, T., Y. L. Hu, F. F. Wang, Z. Chen, and J. Wu, Is there any difference in local time variation in ionospheric F2-layer disturbances between earthquake-induced and Q-disturbance events?, *Annales Geophysicae*, *33*, 687–695, doi:10.5194/angeo-33-687-2015, 2015.

Yizengaw, E., M. B. Moldwin, D. Galvan, B. A. Iijima, A. Komjathy, and A. J. Mannucci, Global plasmaspheric TEC and its relative contribution to GPS TEC, *Journal of Atmospheric and Solar-Terrestrial Physics*, *70*, 1541–1548, doi:10.1016/j.jastp.2008.04.022, 2008.

Yue, X., W. S. Schreiner, D. C. Hunt, C. Rocken, and Y.-H. Kuo, Quantitative evaluation of the low Earth orbit satellite based slant total electron content determination, *Space Weather*, *9*, 09001, doi:10.1029/2011SW000687, 2011.

Zhang, M.-L., L. Liu, W. Wan, and B. Ning, Comparison of the observed topside ionospheric and plasmaspheric electron content derived from the COSMIC podTEC measurements with the IRI_Plas model results, *Advances in Space Research*, *60*, 222–227, doi:10.1016/j.asr.2016.10.025, 2017.